Study of multiparticle production in Reggeon field theory

J. Bartels* and E. Rabinovici
Fermi National Accelerator Laboratory,† Batavia, Illinois 60510
(Received 17 September 1975)

The concept of Reggeon field theory (RFT) is applied to particle production in the multi-Regge region. For processes with repeated Pomeron ($\tilde{P}$) exchange we calculate the high-energy behavior of the production cross sections $\sigma_n(s)$ and find that $\sigma_n(s) \sim \sigma_{el}(s) \sim (\ln s)^{-5/6}$ for every n. It is then shown that s-channel unitarity constraints are respected: in the absence of $\tilde{P}$ cuts these processes are known to violate the Froissart bound (Finkelstein-Kajantie problem). We show that the inclusion of $\tilde{P}$ cuts in our RFT model solves this problem, provided the $\tilde{P}$-particle-$\tilde{P}$ vertex is not large. Furthermore, we demonstrate that the way in which s-channel unitarity is restored does not lead to decoupling problems. Finally, particle production with a secondary Reggeon exchange is considered. We find that the $\sigma_n(s)$ have qualitatively the same behavior as in the absence of $\tilde{P}$ cuts.

I. INTRODUCTION

The problem of formulating a consistent theory that describes the high-energy small-momentum-transfer limit of hadronic scattering and accommodates a nonvanishing total cross section has survived many attempted solutions. Recently the existence of a strong-coupling solution in Reggeon field theory (RFT)[1,2] has stimulated a new series of investigations, and many facets of RFT have been studied, related to both diffractive and nondiffractive properties.[3]

By their very construction, RFT's satisfy t-channel unitarity, but although they involve multi-Pomeron cuts which have been used in absorptive models[4-6] to enforce s-channel unitarity, it is not *a priori* clear that they obey all s-channel requirements. In the absence of a complete proof of s-channel unitarity, one is led, as a first step, to check whether RFT at least satisfies some of the constraints imposed by unitarity. The conventional Regge-pole model has been shown to be inconsistent with unitarity in various inelastic processes,[7] and it is natural to test RFT in the very same reactions. Such a test has been performed for the triple-Regge region,[8] and all inconsistencies were found to be removed in RFT.[9] In this paper we study another pitfall of Regge-pole models, multiparticle production processes with repeated Pomeron exchange. It has been known for many years[10,11] that in these processes a Pomeron pole with intercept 1 leads to a violation of the Froissart bound.

Our interest in multiparticle production processes is not only restricted to the test of s-channel unitarity constraints. One of the major problems that have to be addressed, once RFT has been proven to pass the most serious tests, is that of how the bare Pomeron and the total cross section are built up. Again, a complete answer to this has not yet been obtained, but a study of multiparticle production processes may provide further insight.

These are the two issues of this paper. The framework of our calculations will be a RFT which is based on the Reggeon calculus for multiparticle production amplitudes derived recently.[12] For processes in which only Pomerons are involved, our RFT coincides with that used by Migdal, Polyakov, and Ter-Martirosyan[1] (MPT), but our formalism is general enough to include secondary trajectories as well. Our main interest is focused onto the integrated partial cross sections $\sigma_n(s)$ rather than the production amplitudes $T_{2\to n}$, and this, as we will show, requires the formulation of a RFT for the $\sigma_n(s)$ directly. In all these calculations we use the linear, self-interacting Pomeron pole with renormalized intercept 1, which has been described in Ref. 2. As has been shown in Ref. 13 this corresponds to the bare intercept being greater than 1.

In the first part of our paper we study the partial cross sections σ_n for multiparticle production with repeated Pomeron exchange. In particular, we want to test whether the Pomeron cuts solve the Finkelstein-Kajantie problem of the simple pole model. In examining the high-energy behavior of $\sigma_n(s)$, we find that for $s \to \infty$ and fixed n

$$\sigma_n(s) \sim \sigma_{el}(s) \tag{1.1}$$

for all n. This result is radically different from the situation in the absence of Pomeron cuts. But it also differs from the result obtained by MPT,[1] who studied the same processes. We show that their result actually represents a nonleading contribution to $\sigma_n(s)$.

In order to prove that these cross sections do not violate s-channel unitarity we first rephrase the problem of the Finkelstein-Kajantie model in terms of a j-plane singularity above $j=1$.[14] We then trace the fate of this singularity in the presence of Pomeron ($\tilde{P}$) cuts. The result is that for

small Pomeron-particle-Pomeron ($\tilde{P}P\tilde{P}$) couplings the singularity disappears. Thus, s-channel unitarity is restored. We find, however, some indications that for larger values of the $\tilde{P}P\tilde{P}$ coupling the singularity may survive.

In the process of restoring s-channel unitarity, the Pomeron cuts produce a softening of the renormalized $\tilde{P}P\tilde{P}$ vertex. From models where the $\tilde{P}P\tilde{P}$ vertex vanishes as a function of the two Pomeron momenta, we know that the Pomeron is forced to decouple from many processes at zero momentum transfer, even from elastic scattering.[15,16] We show that in RFT the $\tilde{P}P\tilde{P}$ vertex is screened in such a manner that decoupling problems do not arise. We do this by studying the $\tilde{P}PR$ (Pomeron-particle-Reggeon) vertex at nonzero values of the Reggeon momentum.

This concludes our consistency tests of processes with repeated Pomeron exchange. As a consequence of (1.1), the sum of these cross sections behaves like $\sigma_{el}(s)$ and is not large enough to account for the total cross section. In fact, when $s \to \infty$, $\sigma_{el}(s)/\sigma_{tot} \to 0$ in RFT.[1,2] This situation has to be confronted with certain absorption models where a consistent theory is formulated to build the total cross section only out of Pomeron-dominated processes.[4,5] Our result implies that one has to consider also production processes with non-Pomeron exchange. We take a simple model where all particles are produced from one secondary Regge pole, but allow for interactions with the self-coupled Pomeron. The main subject we are interested in is the question to what extent the presence of cuts changes the behavior of $\sigma_n(s)$. It turns out that, unlike the previous case, the cross sections are qualitatively unchanged by the presence of cuts. We discuss the relevance of this result.

Our paper will be organized as follows: We begin in Sec. II with the description of a simple model whose properties are similar to those of the RFT model to be considered later and will serve as a useful guide in understanding our results. In Sec. III we describe the formalism of RFT that we will use later on. In particular, we will explain why we need a special RFT for the cross sections and cannot proceed in the way of MPT.[1] Sections IV, V, and VI are devoted to processes with repeated Pomeron exchange. In Sec. IV we compute the high-energy behavior of $\sigma_n(s)$. This requires some calculations, and we divide the section into two parts: The first will contain all the technical details, and in the second half we present and discuss the results. Section V contains the proof that the Froissart bound is satisfied and in Sec. VI we make sure that decoupling problems are avoided. In Sec. VII we consider processes with a secondary Reggeon. We conclude our paper with a summary of results.

II. MULTIPARTICLE PRODUCTION: A SIMPLE MODEL

In this section we consider a simple model for multiparticle production with repeated Pomeron exchange. It will turn out that many features of this simple model will survive in the RFT of the following sections. We will, therefore, use this consideration as a guide in understanding the situation in more sophisticated models.

Let us consider the following structure for the cross sections $\sigma_n(Y)$, associated with the processes shown in Fig. 1:

$$\sigma_n(Y) = \text{const} \times U^{n-2} \int \prod_{i=1}^{n-1} \left(\frac{dy_i}{y_i^{1+p}} \right) \delta \left(Y - \sum_{i=1}^{n-1} y_i \right), \tag{2.1}$$

where $Y = \ln s$ and y_i are total rapidity and the rapidity gaps between the produced particles, respectively. The constant U is proportional to the square of the $\tilde{P}P\tilde{P}$ vertex. This factorized form of the production cross section is obtained if we take the Pomeron to be a simple moving pole with intercept 1 and integrate over the momentum transfers t_i. For reasons which will become clear later we generalize the number of transverse directions to be D ($D=2$ is the physical dimension). For each t_i integration, we then have an additional factor $t_i^{\,p}$ with $p = \frac{1}{2}D - 1$. (Alternatively, such a factor $t_i^{\,p}$ could reflect a dynamical softening of the $\tilde{P}P\tilde{P}$ vertex.) In the following, we will call this the Finkelstein-Kajantie model in D dimensions. *It will turn out that RFT at $D=2$ will have the same qualitative features as this simple model at D greater than 2.*

One may try to evaluate the asymptotic energy behavior of (2.1) by scaling the rapidities:

$$x_i = y_i / Y . \tag{2.2}$$

This leads to

$$\sigma_n(Y) = \text{const} \times \frac{U^{n-2}}{Y^{1+(n-1)p}} \times \int_0^1 \prod_{i=1}^{n-1} dx_i \, \delta \left(1 - \sum_{i=1}^{n-1} x_i \right) \frac{1}{x_i^{1+p}} . \tag{2.3}$$

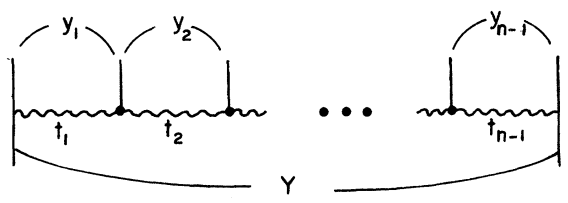

FIG. 1. Repeated Pomeron exchange without cut corrections.

The power of Y in front of the integral will indicate the correct asymptotic behavior of σ_n only as long as the integral is a finite constant. In this case one finds that

$$\sigma_n(Y) = \text{const} \times \frac{U^{n-2}}{Y^{1+(n-1)p}} \tag{2.4}$$

and

$$\frac{\sigma_{n+1}(Y)}{\sigma_n(Y)} \sim \frac{U}{Y^p} \ . \tag{2.5}$$

However, the x_i integrations in (2.3) diverge at $x_i = 0$, and the integral, therefore, will strongly depend on how we define the lower limit of the rapidity integrations. For example, if we require that all subrapidities become large when $s \to \infty$, say

$$y_i \geq C Y^q, \quad 0 < q \leq 1 \ , \tag{2.6}$$

then the asymptotic behavior of (2.3) becomes

$$\sigma_n(Y) \sim U^{n-2} \times \begin{cases} Y^{-1-p-(n-2)qp} & \text{if } 0 < p < 1 \\ Y^{-1}(\ln Y)^{n-2} & \text{if } p = 0 . \end{cases} \tag{2.7}$$

For $q = 1$, this agrees with (2.4) (except when $p = 0$), but (2.7) shows that the decrease of $\sigma_n(Y)$ as a function of s becomes smaller and smaller, when q approaches zero, and in the limit $q = 0$, the asymptotic behavior of $\sigma_n(Y)$ is

$$\sigma_n(Y) \sim U^{n-2} \times \begin{cases} Y^{-1-p}, & 0 < p < 1 \\ Y^{-1}(\ln Y)^{n-2}, & p = 0 . \end{cases} \tag{2.8}$$

Let us first consider $p \neq 0$. Then (2.8) tells us that

$$\sigma_n(Y) \sim \sigma_{\text{el}}(Y) \tag{2.9}$$

for all n. This means that the region of phase space $y_i \geq cY$, which leads to (2.4) is far from giving the leading contribution to $\sigma_n(Y)$. In fact, the behavior (2.7) or (2.8) comes from the *small* x region in (2.3) which implies that in the most favored contribution to σ_n all but one rapidity is finite (they may still be large but do not increase with energy). In order to see how this is related to the contribution (2.3), we keep nonleading terms in (2.8):

$$\sigma_n \sim U^{n-2} Y^{-1-p} [c_{n1} + c_{n2} Y^{-p} + \cdots + c_{n\,n-1} Y^{-(n-2)p}] \tag{2.10}$$

(c_{ij} are some combinatorial constants). In the first term [which is (2.8)], all x but one are small; in the second all but two, and so forth, until in the last term [which is (2.3)] all x are staying away from its lower limit. Thus, (2.10) can be considered as an expansion in the number of large rapidity gaps. For the case $p = 0$ we only note that the situation is quite different, and in the leading contribution (2.8) none of the rapidity gaps is driven to its lower limit.

It is important to note that in (2.3) the divergence of the x_i integration at the lower end is closely related to the large-t_i behavior. In performing the t_i integration which then resulted in (2.1) we neglected any t_i dependence of the vertices which would have led to a cutoff of large t_i values. As a consequence of this, the y_i integration required a cutoff for small values. If we would, instead of this, have included a more realistic exponential damping of the $\tilde{P}P\tilde{P}$ vertex (or simply have cut off the t_i integration), then the remaining y_i integrations would no longer diverge. The results on the behavior of σ_n would not change. However, it is important to keep in mind that such a crude approximation of the t_i dependence, as we made in (2.1), makes the y_i integration infrared divergent.

After finding the asymptotic behavior of $\sigma_n(s)$, one might try to take a glimpse at the nature of the total cross section resulting from these processes. Although it is known that the behavior of $\sigma_n(s)$ in the $(n, \ln s)$ plane may be nonuniform, we do this by summing over the leading terms of $\sigma_n(s)$. For the moment we are interested only in a heuristic argument, and that the conclusions made from this are correct will be shown later on. For the case $0 < p < 1$, Eq. (2.10) suggests that, as long as U is small enough, the sum over the leading terms will converge, and the resulting σ_{tot} behaves like $\sigma_{\text{el}} \sim Y^{-1-p}$. However, when U is large, the sum starts to diverge, indicating that the asymptotic behavior of σ_{tot} is stronger than σ_{el}. In particular, a power of s might be built up which violates the Froissart bound. For $p = 0$, σ_{tot} goes like $s^\alpha (\alpha > 0)$ for any nonzero $\tilde{P}P\tilde{P}$ coupling, which is another way of stating the Finkelstein-Kajantie problem. In Sec. V, we will present a more rigorous treatment of this problem.

The model which we have discussed in this section seems oversimplified compared to RFT. Nevertheless, some of its qualitative features will survive and the preceding discussion will help us to understand the situation in RFT. In particular, we will find a strong similarity between RFT and our model for $2 < D < 4$, i.e., $0 < p < 1$. The most distinctive feature of this model is that in the leading contribution (2.8) to the high-energy behavior, $n-2$ of the $n-1$ rapidity gaps prefer to be finite, thus excluding an n dependence of the asymptotic behavior of σ_n. This was related to the possibility of divergences at small rapidity gaps, and the divergences were the result of disregarding the large t damping properties of the vertices. Being aware of this problem we now turn to RFT in production processes.

III. RFT IN PRODUCTION PROCESSES

In this section we give a description of RFT in production processes. We are mainly interested in production processes with repeated Pomeron exchange, but we will formulate the rules general enough to include non-Pomeron Reggeons as well.

The basis of our RFT is the Reggeon calculus for production processes which has been derived in Ref. 12. It is the equivalent of Gribov's Reggeon calculus for the $2\to 2$ scattering and exhibits many properties that one expects on general grounds. In particular, it is in agreement with the energy discontinuity structure required by the Steinmann relations and, when continued to the physical region of the crossed channels, exhibits the main features of physical partial-wave amplitudes. The transition from the Reggeon calculus to RFT proceeds in the same way as in the $2\to 2$ scattering case. Since one is interested only in those specific points of (angular momentum, transverse momentum) space, where an accumulation of j-plane singularities takes place, one approximates all quantities appearing in the Reggeon calculus (vertex functions, propagators, and signature factors) by their behaviors near this accumulation point. As a result of this, one is left with a local field theory. As compared to the elastic case, there is only one new feature one has to observe in deriving RFT from the Reggeon calculus for production processes. This is the fact that because of the Steinmann relations the $T_{2\to n}$ amplitude cannot be written as just one multiple Sommerfeld integral, but is a sum of different terms, each of them reflecting an allowed set of simultaneous discontinuities. Only when making approximations in the spirit of RFT, this sum of terms may collapse, and one is left with a smaller number of terms. In the particular case of only Pomerons it happens that, for any number of produced particles, all terms are combined to one single term:

$$T_{2\to n}(y_1,\cdots,y_{n-1},\vec{q}_1,\cdots,\vec{q}_{n-1}) = \frac{(i)^{n-1}s}{(2\pi i)^{n-1}}\int dE_1\cdots dE_{n-1}\, e^{-y_1E_1}\cdots e^{-y_{n-1}E_{n-1}}F_n(E_1,\cdots,E_{n-1},\vec{q}_1,\cdots,\vec{q}_{n-1}). \tag{3.1}$$

The partial wave F_n is the object for which RFT is formulated. In (3.1), we have used $E_i = 1 - j_i$, where j_i is the angular momentum in the t_i channel, $\vec{q}_i^{\,2} = -t_i$ the momentum transfer, and y_i the rapidity gap (Fig. 1). The factor i^{n-1} in front of the integral is the result of approximating signature factors. The η variables (Toller angles), whose singularity structure is correctly described by the Reggeon calculus, do not explicitly appear in (3.1), but F_n depends on them through $\vec{q}_i\cdot\vec{q}_j$. The remaining part of the η dependence is, together with some phase factors, absorbed into an effective complex-valued $\tilde{P}P\tilde{P}$ coupling constant. The Feynman rules for a diagram of the partial wave F_n can be formulated as follows (Fig. 2):

(a) Define a direction, say from the left to the right.

(b) $E_i, \vec{q}_i$ are the sums of Reggeon energies and momenta in the t_i channel (marked by the vertical cut in Fig. 2). In order to maintain energy and momentum conservation everywhere in a diagram, each produced particle carries away energy and momentum $E_i - E_{i+1}$, $\vec{q}_i - \vec{q}_{i+1}$.

(c) Put a number V_0 at the $\tilde{P}P\tilde{P}$ vertex (V_0 is generally complex) and conserve energy and momentum.

(d) For all other parts of the diagram use the rules of the $2\to 2$ RFT.[2]

Introducing a field operator $\psi(\vec{x},t)$ for the Pomeron (and $\psi^\dagger$ for its Hermitian conjugate), the cou-

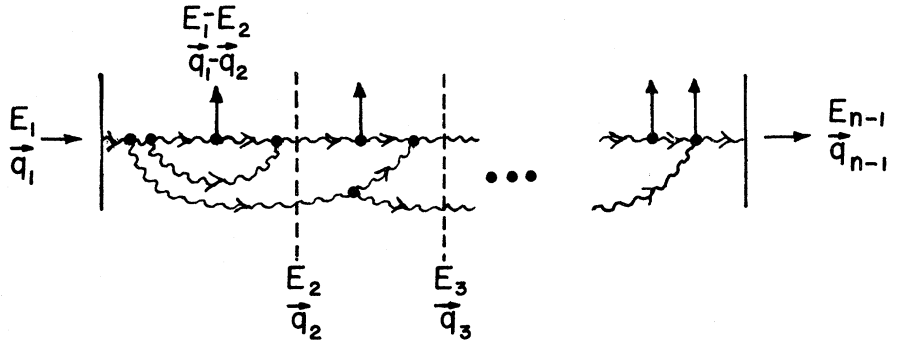

FIG. 2. Feynman rules for the Reggeon calculus of the production amplitude.

pling to the produced particle is described by a source operator. For example, the nonamputated $\tilde{P}P\tilde{P}$ vertex is

$$\langle 0|\psi^\dagger(\vec{x}_1 t_1)\,\psi(\vec{x}_2 t_2)\,V_0\psi^\dagger(\vec{x}_2 t_2)\,\psi(\vec{x}_3 t_3)|0\rangle\ . \qquad (3.2)$$

A derivation of these rules has been given in the final section of the second paper of Ref. 12. They coincide with those used by MPT. We further mention that for the case when a secondary Reggeon is included the rules (a)–(d) remain unchanged. In Sec. VII, we will consider particle production from one secondary Reggeon, together with absorptive Pomeron cuts. We than use (a)–(d) together with (3.1). The only change is the replacement in (3.1): $(i)^{n-1} \to \xi_{\alpha(0)}{}^{n-1}$, with $\alpha(0)$ being the intercept of the secondary Reggeon.

In the following we concentrate on processes with only Pomerons. If we allow only for fully enhanced diagrams, the Lagrangian for F_n is given by

$$\mathcal{L} = \mathcal{L}_0 + \psi^\dagger V_0\psi + J^\dagger\psi^\dagger + J\psi - \tfrac{1}{2}ig_0\,\psi^\dagger\psi(\psi+\psi^\dagger) \qquad (3.3)$$

with

$$\mathcal{L}_0 = \tfrac{1}{2}i\,\psi^\dagger\overleftrightarrow{\partial}_t\psi - \alpha_0'\,\nabla\psi^\dagger\cdot\nabla\psi - \Delta_0\psi^\dagger\psi\,. \qquad (3.4)$$

The first term $\mathcal{L}_0$ describes the propagation of the free Pomeron, $J\psi$ and $J^\dagger\psi^\dagger$ couple the Pomeron to the incoming particles, and the source term $\psi^\dagger V_0\psi$ attaches the produced particles to the Pomeron. The last term in (3.3) induces the Pomeron self-interaction, leading to absorptive corrections. Without this triple coupling, we would have just the diagram of Fig. 1. Including g_0 generates those of Fig. 3. Looking at this figure, we recognize three effects of Pomeron cuts: (i) The Pomeron propagator becomes renormalized [Fig. 4(a)]. Since this is independent of the particle production, it is the same as described by Abarbanel and Bronzan[2] for the elastic scattering. (ii) The $\tilde{P}P\tilde{P}$ vertex (i.e., the source operator $\psi^\dagger V_0\psi$) undergoes a renormalization [Fig. 4(b)]. (iii) Particles are produced out of different Pomeron lines [Fig. 4(c)]. It will turn out that these contributions are suppressed at large energies.

Before we plunge into calculations it is necessary to hesitate for a moment and to recall our experience from the previous section. So far we have been describing the RFT for the production

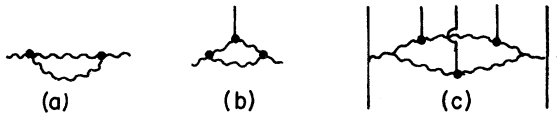

FIG. 4. Effects of absorptive cuts in the production amplitude: (a) renormalization of the Pomeron, (b) renormalization of the $\tilde{P}P\tilde{P}$ vertex, (c) Particle production from different Pomeron lines.

amplitude $T_{2\to n}$, but what we are really interested in are the cross sections σ_n. Naively, we would go ahead and compute $T_{2\to n}$, then square it and integrate over rapidities and transverse momenta of the produced particles. This, however, is somewhat dangerous. For from what we learned in Sec. II, it follows that, since we have approximated all vertices by constants (i.e., we have no damping coming from the large-t behavior of the vertices), the rapidity integration will diverge. We have demonstrated this in (2.1) for the diagrams of Fig. 1, which are described by our Lagrangian (3.3) without Pomeron self-interaction. In order to obtain the correct asymptotic behavior of the σ_n, we had to introduce a low-energy cutoff for the y integration, and the evaluation of the integrals was possible only because we knew the dependence on each rapidity separately. Using RFT for $T_{2\to n}$, one usually obtains a scaling law which does not give enough information to proceed in the same way. We will, therefore, proceed in a slightly different manner.

The idea is the following: Let us take a diagram that contributes to $T_{2\to n}$ and close it on itself. As an example, the square of Fig. 1 is shown in Fig. 5. The result of this looks very much like a Reggeon diagram for the $2\to 2$ scattering amplitude. In particular, a quartic coupling arises as the square of the production vertex. This consideration holds for any diagram of $T_{2\to n}$ (in fact, not only for squares of diagrams but also for interference terms), and

$$\sigma_n = \int d\Omega_n\, T_{2\to n}\, T^*_{2\to n}$$

can be written as a sum of a specific class of diagrams for the $2\to 2$ process. Each of these graphs has, of course, still the divergences mentioned

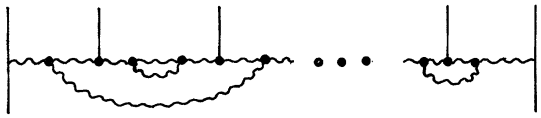

FIG. 3. Repeated Pomeron exchange with cut corrections.

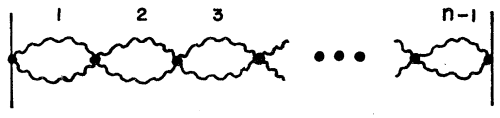

FIG. 5. A Reggeon diagram for $\sigma_n(E)$, resulting from squaring the diagram of Fig. 1.

above, but now we can employ the methods of field theory[17] to regularize divergent integrations. That this leads to the correct results for σ_n can easily be checked for the simple diagrams of Fig. 5.

We finally want to demonstrate how the $2 \to 2$ Reggeon calculus for σ_n can formally be derived. Let us take the $2 \to 3$ process. Then the cross section σ_3 is

$$\sigma_3(Y) = \frac{N}{s^2} \int dy_1 dy_2 \, \delta(Y - y_1 - y_2) \int d^2q_1 d^2q_2 \, T_{2\to 3}(y_1, y_2, \vec{q}_1, \vec{q}_2) \, T^*_{2\to 3}(y_1, y_2, \vec{q}_1, \vec{q}_2) \, , \tag{3.5}$$

with N being a normalization constant and $T_{2\to 3}$ as given by (3.1):

$$T_{2\to 3}(y_1, y_2, \vec{q}_1, \vec{q}_2) = i^2 s \int \frac{dE_1 \, dE_2}{(2\pi i)^2} \, e^{-y_1 E_1} e^{-y_2 E_2} F_3(E_1, E_2, \vec{q}_1, \vec{q}_2) \, . \tag{3.6}$$

The complex conjugate to $T_{2\to 3}$ is obtained by taking the complex conjugate of the signature factors, which in (3.6) appear in the factor i^2 and the complex-valued $\tilde{P}P\tilde{P}$ coupling V_0 in $F_{2\to 3}$. Therefore,

$$T^*_{2\to 3}(y_1, y_2, \vec{q}_1, \vec{q}_2) = (-i)^2 s \int \frac{dE_1' \, dE_2'}{(2\pi i)^2} \, e^{-y_1 E_1'} e^{-y_2 E_2'} F_3(E_1', E_2', \vec{q}_1, \vec{q}_2) \Big|_{V_0 \to V_0^*} \, . \tag{3.7}$$

We insert this together with (3.6) into (3.5), in $T^*_{2\to 3}$ replace $\vec{q}_1, \vec{q}_2$ by $-\vec{q}_1, -\vec{q}_2$ (T is invariant under this transformation), and perform the y_1 and y_2 integrations. This leads to δ functions between Reggeon energies of $T_{2\to 3}$ and $T^*_{2\to 3}$ and allows us to integrate over E_1' and E_2'. The final answer for σ_3 is

$$\sigma_3(Y) = N \int \frac{dE}{2\pi i} \, e^{-YE} \int \frac{d\omega_1 \, d\omega_2}{(2\pi i)^2} \, F_{2\to 3}(\omega_1, \omega_2, \vec{q}_1, \vec{q}_2) \, F_{2\to 3}(E - \omega_1, E - \omega_2, -\vec{q}_1, -\vec{q}_2) \, . \tag{3.8}$$

This has exactly the form of RFT for the $2 \to 2$ amplitude with Reggeon energy E and momentum transfer zero (Fig. 6) and holds for any contribution to $F_{2\to 3}$. We therefore define a Sommerfeld-Watson transform $\sigma_3(E)$:

$$\sigma_3(Y) = \frac{1}{2\pi i} \int dE \, e^{-YE} \sigma_3(E) \, , \tag{3.9}$$

and for the computation of $\sigma_3(E)$ we can use the Reggeon calculus (and RFT) of the $2 \to 2$ amplitude. As to the topology of diagrams for $\sigma_3(E)$, a quartic coupling appears as the product of the $\tilde{P}P\tilde{P}$ vertex in $T_{2\to 3}$ and $T^*_{2\to 3}$: It is $U_0 = V_0 V_0^*$ and hence real.

This consideration holds for all $\sigma_n(Y)$, and the diagrams for $\sigma_n(E)$ are obtained by squaring those of $T_{2\to n}$ (Fig. 7). The Lagrangian which generates all these diagrams is

$$\mathcal{L} = \sum_{i=1,2} [\mathcal{L}_{0i} - \tfrac{1}{2} i g_0 \psi_i^\dagger \psi_i (\psi_i^\dagger + \psi_i)] - U_0 \psi_1^\dagger \psi_1 \psi_2^\dagger \psi_2 + J \psi_1 \psi_2 + J^\dagger \psi_1^\dagger \psi_2^\dagger \, . \tag{3.10}$$

The reason why we need two Pomeron fields ψ_1 and ψ_2 is that we allow for Pomeron self-interactions in the lower and upper half of Fig. 7, but the only place where ψ_1 and ψ_2 may come into contact are the quartic vertex U_0 and the coupling to the external particles $J\psi_1\psi_2$. [Note that these are not all the diagrams which would arise in a RFT with a full quartic interaction (e.g., the diagrams of Fig. 8 do not appear in our theory). We have only those diagrams which arise from squaring $T_{2\to n}$.] With the Lagrangian (3.10), $\sigma_n(E)$ is given by the sum of all diagrams which are proportional to U^{n-2}.

This completes the description of RFT for production processes. We still want to mention that the Reggeon calculus for σ_n, which we have derived here only for a pure Pomeron theory, remains valid when other Reggeons are included. The main reason is that in multiplying $T_{2\to n}$ with its complex conjugate and integrating over the physical region of the produced particles, the whole phase structure which makes $T_{2\to n}$ that complicated, always becomes very simple: The phase factors can be absorbed into the quartic coupling, which is the product of two complex-conjugate numbers and therefore real.

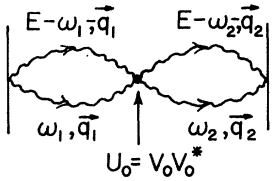

FIG. 6. A Reggeon diagram for $\sigma_3(E)$.

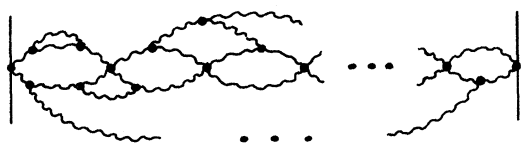

FIG. 7. A RFT contribution to $\sigma_n(E)$.

FIG. 8. Quartic interactions that do not occur in our RFT for σ_n.

IV. HIGH-ENERGY BEHAVIOR OF $\sigma_n(Y)$

We now turn to the high-energy behavior of the production cross sections $\sigma_n(Y)$ for fixed n. The Lagrangian for these cross sections is given by (3.10), whereas the production amplitudes are described by the Lagrangian (3.3). The asymptotic behavior of $\sigma_n(Y)$ as a function of Y is controlled by the infrared structure of its Sommerfeld-Watson transform $\sigma_n(E)$. In order to evaluate the infrared behavior of $\sigma_n(E)$ we first define the generating function

$$\sigma(E) - \sum_n \sigma_n(E), \tag{4.1}$$

with $\sigma_n(E)$ being proportional to U^{n-2}:

$$\sigma_n(E) = U^{n-2}\tilde{\sigma}_n(E) . \tag{4.2}$$

We find a renormalization-group equation (RGE) for $\sigma(E)$, expand the solution in powers of U, and then determine the infrared behavior of the coefficient functions $\tilde{\sigma}_n(E)$. In addition to that, in order to see the relation between the behavior of the cross sections $\sigma_n(Y)$ and the amplitudes $T_{2\to n}$, we first consider the infrared behavior of the renormalized $\tilde{P}P\tilde{P}$ vertex and derive a scaling law for $T_{2\to n}$.

In order to make the reading as easy as possible, we organize this section in two parts. In part A, we derive and discuss the RGE's together with its formal solutions. In part B, we present and discuss the results and the physical implications.

A. Calculations

As we have said before, one of the effects of $\tilde{P}$ cuts in production processes is the renormalization of the $\tilde{P}P\tilde{P}$ vertex. We, therefore, first consider the infrared behavior of the renormalized amputated $\tilde{P}P\tilde{P}$ vertex $\Gamma_{\tilde{P}P\tilde{P}}(E_i, \vec{k}_i)$ [Fig. 9(a)]. In order to make our calculations self-contained, we start by reviewing the results of Ref. 2 on the Pomeron self-interaction. The renormalized inverse propagator Γ^{11} [Fig. 9(b)],

$$\Gamma^{11} = Z_1 \Gamma^{11}_{\text{unren}} , \tag{4.3}$$

satisfies the conditions

$$\Gamma^{11}(E, \vec{k}, \alpha', g, E_N)\Big|_{\substack{E=0 \\ \vec{k}=0}} = 0 , \tag{4.4}$$

$$\frac{d}{dE}\, i\Gamma^{11}(E, \vec{k}, \alpha', g, E_N)\Big|_{\substack{E=-E_N \\ \vec{k}=0}} = 1 , \tag{4.5}$$

$$\frac{d}{d\vec{k}^2}\, i\Gamma^{11}(E, \vec{k}, \alpha', g, E_N)\Big|_{\substack{E=-E_N \\ \vec{k}=0}} = -\alpha' \tag{4.6}$$

The renormalized coupling constant g is given by the amputated three-point function [Fig. 9(c)]:

$$\Gamma^{12} = Z_1^{3/2}\, \Gamma^{12}_{\text{unren}} , \tag{4.7}$$

$$\Gamma^{12}_R(E_i, \vec{k}_i, \alpha', g)\Big|_{\substack{E_1=2E_2=2E_3=-E_N \\ \vec{k}_i=0}} = \frac{g_d}{(2\pi)^{(D+1)/2}} . \tag{4.8}$$

In (4.8) g carries a subscript "d" indicating that it still has dimensions. We introduce a dimensionless coupling g through

$$g = g_d \frac{E_N^{D/4-1}}{\alpha'^{D/4}} . \tag{4.9}$$

The RGE for Γ^{11} has the form

$$[\xi\partial_\xi - \beta_g\partial_g - (\zeta - \alpha')\partial_{\alpha'} - 1 + \gamma_1] \times \Gamma^{11}(\xi E, \vec{k}, \alpha', g, E_N) = 0 , \tag{4.10}$$

with

$$\beta_g = E_N \partial_{E_N} g(E_N) , \tag{4.11}$$

$$\zeta = E_N \partial_{E_N} \alpha'(E_N) , \tag{4.12}$$

$$\gamma_1 = E_N \partial_{E_N} \ln Z_1(E_N) . \tag{4.13}$$

The solution ($t = \ln\xi$) to (4.10) is

$$\Gamma^{11}(\xi E, \vec{k}, \alpha', g, E_N) = \exp\left\{\int_{-t}^{0} [1 - \gamma_1(g(t'))]\, dt'\right\} \times \Gamma^{11}(E, \vec{k}, \alpha'(-t), g(-t), E_N) . \tag{4.14}$$

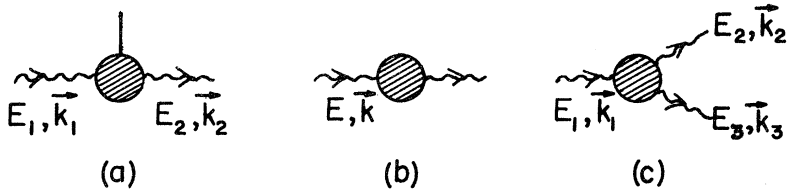

FIG. 9. Green's functions that are computed in Sec. IIA: (a) the $\tilde{P}P\tilde{P}$ vertex, (b) the Pomeron propagator, (c) the triple-Pomeron vertex function.

In lowest order ϵ, one finds an infrared-stable fixed point $\bar{g}$ for g, such that for $t \to -\infty$, $g(-t) \to \bar{g}$. For $\alpha'(-t)$ one finds

$$\alpha'(-t) = \alpha' \xi^{-z} . \tag{4.15}$$

At the fixed point $\bar{g}$, the values for γ_1 and z are

$$\gamma_1 = -\frac{\epsilon}{12} , \quad z = 1 + \frac{\epsilon}{24} . \tag{4.16}$$

Now we consider the renormalized $\tilde{P}P\tilde{P}$ vertex $\Gamma_{\tilde{P}P\tilde{P}}$ [Fig. 9(a)],

$$\Gamma_{\tilde{P}P\tilde{P}} = Z_4^{-1} \Gamma_{\tilde{P}P\tilde{P};\text{unren}} , \tag{4.17}$$

where Z_4 combines the renormalization constant of the source operator $\psi^\dagger V_0 \psi$ and the wave-function renormalization of the external Pomeron lines. Z_4 is defined through

$$\Gamma_{\tilde{P}P\tilde{P}}(E_1, E_2, \vec{k}_1, \vec{k}_2, \alpha', g, E_N)\Big|_{E_1 = E_2 = -E_N ,\ \vec{k}_i = 0} = 1 , \tag{4.18}$$

which indicates that we have taken out V_0 as an over-all constant factor to $\Gamma_{\tilde{P}P\tilde{P}}$. Further, (4.18) tells that $\Gamma_{\tilde{P}P\tilde{P}}$ depends only on two parameters, the triple-Pomeron coupling and the Pomeron slope. Both of them are defined above. The RGE for $\Gamma_{\tilde{P}P\tilde{P}}$ is

$$[\xi \partial_\xi - \beta_g \partial_g - (\zeta - \alpha')\partial_{\alpha'} - \gamma_4] \times \Gamma_{\tilde{P}P\tilde{P}}(\xi E_i, \vec{k}_i, g, \alpha', E_N) = 0 , \tag{4.19}$$

with

$$\gamma_4 = E_N \partial_{E_N} \ln Z_4 . \tag{4.20}$$

The solution to (4.19) is

$$\Gamma_{\tilde{P}P\tilde{P}}(\xi E_i, \vec{k}_i, g, \alpha', E_N) = \exp\left[+\int_{-t}^{0} dt' \, \gamma_4(g(t'))\right] \Gamma_{\tilde{P}P\tilde{P}}(E_i, \vec{k}_i, g(-t), \alpha'(-t), E_N) . \tag{4.21}$$

The only new quantity is $\gamma_4(g)$. In lowest order ϵ, only the diagram of Fig. 4(b) contributes. Inserting the fixed-point value for g, we obtain

$$\gamma_4(\bar{g}) = \beta = \epsilon/6 . \tag{4.22}$$

Since in our notation [cf. (4.18)] $\Gamma_{\tilde{P}P\tilde{P}}$ is dimensionless and, hence, depends only on dimensionless quantities, $\Gamma_{\tilde{P}P\tilde{P}}$ on the right-hand side of (4.21) can be written as

$$\Gamma_{\tilde{P}P\tilde{P}}\left(\frac{E_i}{E_N} , \frac{\alpha'(-t)\vec{k}_i \cdot \vec{k}_i}{E_N} , g(-t), 1, 1\right) . \tag{4.23}$$

In the limit $\xi \to 0$ ($t \to -\infty$) we obtain, using (4.15) for $\alpha'(-t)$,

$$\Gamma_{\tilde{P}P\tilde{P}}(\xi E_i, \vec{k}_i, g, \alpha', E_N) \underset{\xi \to 0}{\sim} \xi^{\gamma_4(\bar{g})} \Gamma_{\tilde{P}P\tilde{P}}\left(\frac{E_i}{E_N} , \xi^{-z} \frac{\alpha' \vec{k}_i \cdot \vec{k}_j}{E_N} , \bar{g}\right) . \tag{4.24}$$

Scaling on both sides the momentum vectors by $\xi^{z/2}$, (4.24) can be written as

$$\Gamma_{\tilde{P}P\tilde{P}}(\xi E_i, \xi^{z/2}\vec{k}_i, g, \alpha', E_N) \underset{\xi \to 0}{\sim} \xi^{\beta} \Gamma_{\tilde{P}P\tilde{P}}\left(\frac{E_i}{E_N} , \frac{\alpha' \vec{k}_i \cdot \vec{k}_j}{E_N} , \bar{g}\right) . \tag{4.25}$$

The important result of (4.25) is that $\tilde{P}P\tilde{P}$ vertex, which in the absence of Pomeron cuts was a nonvanishing constant, is now screened and vanishes as $\xi \to 0$ [note that $\beta > 0$ from (4.22)].

In the same way one derives scaling laws for the Pomeron–n-particle–Pomeron vertex ($\tilde{P}nP\tilde{P}$) [Fig. 10(a)]. With the definition

$$\Gamma_{\tilde{P}nP\tilde{P}} = Z_4^{-n} Z_1^{1-n} \Gamma_{\tilde{P}nP\tilde{P};\text{unren}} , \tag{4.26}$$

the result is

$$\Gamma_{\tilde{P}nP\tilde{P}}(\xi E_i, \xi^{z/2}\vec{k}_i, g, \alpha', E_N) \underset{\xi \to 0}{\sim} \xi^{n\beta + (n-1)(\gamma_1 - 1)} \Gamma_{\tilde{P}nP\tilde{P}}\left(\frac{E_i}{E_N} \frac{\alpha' \vec{k}_i \cdot \vec{k}_j}{E_N} , \bar{g}, 1, 1\right) . \tag{4.27}$$

In order to obtain a scaling law for the physical partial wave F_n, we observe that in the leading contribution only one Pomeron couples to the incoming particles,[18] such as illustrated in Fig. 10(b). The expression for the partial wave F_n is then

$$F_{n+2}(E_i, \vec{k}_i) = N_1[\Gamma^{11}(E_1, \vec{k}_i)]^{-1} V_0^n \Gamma_{\tilde{P}nP\tilde{P}}(E_i, \vec{k}_i)[\Gamma^{11}(E_{n+1}, \vec{k}_{n+1})]^{-1} N_1 . \tag{4.28}$$

Formula (4.27) yields the scaling law for F_{n+2}:

$$F_{n+2}(\xi E_i, \vec{k}_i) \underset{\xi \to 0}{\sim} \xi^{n\beta + (n+1)(\gamma_1 - 1)} \Phi_{n+2}\left(\frac{E_i}{E_N} , \xi^{-z} \frac{\alpha' \vec{k}_i \cdot \vec{k}_j}{E_N}\right) . \tag{4.29}$$

Transforming via (3.1) to rapidities, we obtain

$$T_{2\to n}(y_i,\vec{k}_i)\underset{y\to\infty}{\sim} sY^{\beta-(n-1)(\beta+\gamma_1)}\int\prod_{i=1}^{n-1}dE_i\,e^{-E_iy_i/Y}\tilde{\phi}_n\left(\frac{E_i}{E_N},\,Y^z\,\frac{\alpha'\vec{k}_i\cdot\vec{k}_j}{E_N}\right)=Y^{\beta-(n-1)(\beta+\gamma_1)}\,T_{2\to n}\left(\frac{y_i}{Y},\,Y^{z/2}\vec{k}_i\right). \tag{4.30}$$

We finally mention that the parameters γ_1, z, and β have been calculated by methods other than the ϵ expansion.[19,20] The values obtained in the high-temperature expansion are

$$\tfrac{1}{2}\leq-\gamma_1\leq1,\quad\tfrac{3}{2}\leq z\leq2,$$
$$\tfrac{1}{3}\leq2\beta+2\gamma_1+z\leq\tfrac{2}{3}. \tag{4.31}$$

After discussing the properties of the production amplitude $T_{2\to n}$, we now turn to the cross section $\sigma(E)$ and its RGE. According to the Lagrangian (3.10), $\sigma(E)$ depends, in addition to (g_1, α_1') and (g_2, α_2') on the renormalized quartic coupling U. The renormalization of g_i, α_i' is independent of U and, hence, the same as described above. For the definition of the renormalized quartic coupling U, we define the amputated Green's function Γ^{22} for the process Pomeron 1 + Pomeron 2 → Pomeron 1 + Pomeron 2 [Fig. 11(a)]

$$\Gamma^{22}=Z_1{}^2\Gamma^{22}_{\text{unren}} \tag{4.32}$$

and set

$$\Gamma^{22}(E_i,\vec{k}_i,\alpha_i',g_i,U,E_N)\Big|_{\substack{E_1=E_2=E_3=E_4=-E_N/2\\ \vec{k}_i=0}}=\frac{iU_d}{(2\pi)^{D+1}}. \tag{4.33}$$

The subscript "d" to U in (4.33) indicates that U_d still has dimensions. A dimensionless quartic coupling is defined by

$$U=U_d\,\frac{E_N{}^{D/2-1}}{\alpha'^{D/2}}. \tag{4.34}$$

Next we have to renormalize the source operator $J\psi_1\psi_2$ and its Hermitian conjugate. To this end we define the amputated-source–two-Pomeron vertex [Fig. 11(b)]:

$$N=Z_N{}^{-1}Z_1{}^{-1}N_{\text{unren}} \tag{4.35}$$

with

$$N(E_1,E_2,\vec{k}_1,\vec{k}_2,g_i,\alpha_i',U,E_N)\Big|_{\substack{E_1=E_2=-E_N/2\\ \vec{k}_i=0}}=1. \tag{4.36}$$

For $\sigma(E)$ [Fig. 11(c)] we need, in addition to a multiplicative renormalization, one (constant) subtraction, which we define by means of

$$\sigma(E)\big|_{E=-E_N}=0. \tag{4.37}$$

We then have the relation

$$\sigma(E)=Z_N{}^{-2}Z_1{}^{-2}[\sigma_{\text{unren}}(E)-\sigma_{\text{unren}}(-E_N)]. \tag{4.38}$$

The RGE for $\sigma(E)$ is

$$\left[E_N\partial_{E_N}+\sum_{i=1,2}[\beta_g\partial_{g_i}+\xi\partial_{\alpha_i'}+\gamma_1(g_i)]+\beta_U\partial_U+2\gamma_N\right]\sigma(E;g_i,\alpha_i',U,E_N)=+\Delta(g_i,\alpha_i',U,E_N), \tag{4.39}$$

with

$$\gamma_N=E_N\partial_{E_N}\ln Z_N, \tag{4.40}$$
$$\beta_U=E_N\partial_{E_N}U(E_N), \tag{4.41}$$
$$\Delta=-Z_N{}^{-2}Z_1{}^{-2}E_N\partial_{E_N}\sigma_{\text{unren}}(-E_N). \tag{4.42}$$

By dimensional analysis of $\sigma(E)$ we find that

$$[\sigma]=E^{-1}k^D, \tag{4.43}$$

which leads to

$$(\xi\partial_\xi+E_N\partial_{E_N}+\alpha_1'\partial_{\alpha_1'}+\alpha_2'\partial_{\alpha_2'}+1)\,\sigma(\xi E,g_i,\alpha_i',U,E_N)=0. \tag{4.44}$$

This together with (4.39) yields

$$\left[\xi\partial_\xi-\sum_{i=1,2}[\beta_g\partial_{g_i}+(\zeta-\alpha_i')\partial_{\alpha_i'}+\gamma_1(g_i)]-\beta_U\partial_U+1-2\gamma_N\right]\sigma(\xi E,g_i,\alpha_i',U,E_N)=\Delta(g_i,\alpha_i',U,E_N). \tag{4.45}$$

The solution to this equation is

$$\sigma(\xi E, g_i, \alpha_i', U, E_N) = \sigma(E, g(-t), \alpha(-t), U(-t), E_N) \exp\left(\int_{-t}^{0} dt'[-1 + 2\gamma_1(g(t')) + 2\gamma_N(g(t'), U(t'))]\right)$$
$$+ \int_{-t}^{0} dt' \Delta(E_N, g(t'), U(t'), \alpha'(t')) \exp\left(\int_{-t'}^{0} [-1 + 2\gamma_1(g(t'')) + 2\gamma_N(g(t''), U(t''))] dt''\right). \quad (4.46)$$

On the right-hand side of this equation, we put $g_1(t) = g_2(t) = g(t)$ [because g_1 and g_2 are renormalized in the same way and the functional form $g(t)$ is the same for both]. The first term on the right-hand side of (4.46) is the usual solution to a homogeneous RGE, and the second is due to the inhomogeneous term of (4.45). What makes the solution of (4.45), despite the inhomogeneity, rather simple, is the fact that Δ, the inhomogeneous term, is a constant with respect to the Reggeon energy ξE. In solving (4.45), the only t dependence of Δ enters through the auxiliary functions $g_i(t)$, $\alpha_i'(t)$, and $U(t)$. This explains (4.46). The functions $g_i(t)$ and $\alpha_i'(t)$ are the same as in (4.10), and the only new function is $U(t)$. U is a quartic coupling, and we know from previous investigations[21,22] that these couplings tend to be infrared free. In order to determine $U(t)$ for our case we look at the β_U function. It has the form

$$\beta_U = rU + O(U^2),$$

with

$$r = \frac{D}{2} - 1 - \frac{D}{2}\frac{\zeta}{\alpha'} + \gamma_1(g_1) + \gamma_1(g_2) + \gamma_4(g_1) + \gamma_4(g_2). \quad (4.47)$$

Inserting for g_1 and g_2 the fixed-point values, this becomes

$$r = \frac{D}{2} z - 1 + 2\gamma_1 + 2\beta. \quad (4.48)$$

These are all quantities known to us, and using the numerical values obtained in the ϵ expansion (4.16), (4.22), or the high-temperature expansion (4.31) we find $r > 0$. For example, in the ϵ expansion:

$$r = 1 - \epsilon/4. \quad (4.49)$$

Thus, the point $U = 0$ is an infrared-stable fixed point, and for small ξ (or $t \to -\infty$) $U(-t)$ has the behavior

$$U(-t) \sim U e^{rt}. \quad (4.50)$$

This result depends mainly on the sign of r, which is a function of z, γ_1, and β. Once these quantities are given (from the ϵ expansion or high-temperature expansion), the evaluation of r involves no further approximation. In Sec. IV B we will find that the sign of r has still another important effect.

Before we go on, a word might be in place about the renormalizability of our theory at $D = 4$. Our RFT for the production amplitude, as given by the Lagrangian (3.3), is renormalizable at $D = 4$ just as is the RFT with a triple-Pomeron interaction for the $2 - 2$ scattering. But the RFT for the cross sections, as written is (3.10), has lost this nice property. In fact, if we were to compute any Green's function away from the infrared limit, which has a quartic coupling in it, we would have to introduce an infinite number of counterterms, depending on U and g_i, in order to avoid infinities. This is again the result of taking constants for all couplings and disregarding damping properties for large t values. However, in the infrared limit it has been shown by Bardeen *et al.*[22] that only a very limited number of interaction operators can possibly play a role, and in our theory it is only the operator $U\psi_1^\dagger \psi_1 \psi_2^\dagger \psi_2$. Now (4.50) shows that this operator goes to zero in the infrared limit, and the quantity r which determines its infrared behavior is given through the quantities z, γ_1, β. Each of them is computed in a theory that is renormalizable $D = 4$. This is why (4.50) is valid even at $D = 4$, and all results of this section can be continued up to $D = 4$.

Our next step is to determine the infrared behavior $\sigma_n(E)$. To this end we expand the right-hand side of Eq. (4.46), which, as it stands, is valid for all t, in powers of U. In doing this we have to

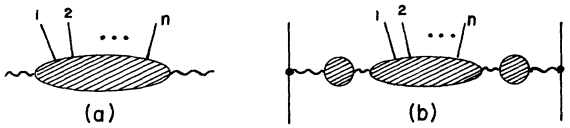

FIG. 10. (a) The $\tilde{P}$-(n-particle)-$\tilde{P}$ vertex, (b) the $2 \to n + 2$ amplitude.

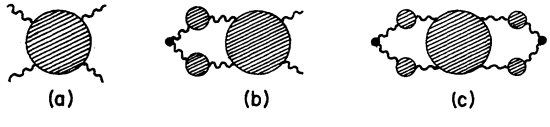

FIG. 11. (a) The 2-Pomeron → 2 Pomeron Green's function Γ^{22}, (b) the coupling to external particles N, (c) the generating function $\sigma(E)$.

assume that this expansion converges, but since our theory is infrared free with respect to U, we can choose our $U=U(0)$ small enough such that a convergent perturbation expansion exists. We then write the left-hand side of Eq. (4.46) as a power series in U [cf. (4.2)], and on the right-hand side we expand all functions in powers of $U(t)$ [the function $U(t)$ depends on U as a boundary value $U(0)=U$]. To simplify our consideration we take $g_1=g_2$ to be the exact fixed-point values, such that the function $g(-t)$ on the right-hand side of (4.46) becomes a constant. (However, our results would be the same if g_1, g_2 are chosen to be near the fixed point.) Equation (4.46) then becomes

$$\sum_n U^n \tilde{\sigma}_{n+2}(\xi E, g, \alpha', E_N) = \sum_n U(-t)^n \tilde{\sigma}_{n+2}(E, g, \alpha'(-t), E_N)\, e^{(2\gamma_1-1)t} \exp\left[\int_{-t}^{0} dt' \sum_n \gamma_{Nn}(g) U(t')^n\right] + \int_{-t}^{0} dt' \sum_n U(t')^n \Delta_{n+2}(g, \alpha'(t'), E_N)\, e^{-(2\gamma_1-1)t'} \exp\left[-\int_{-t'}^{0} dt'' \sum_n \gamma_{Nn}(g) U(t'')^n\right]. \tag{4.51}$$

The remaining t dependence of $\tilde{\sigma}_n$ and Δ_n can be extracted by use of dimensional arguments:

$$\tilde{\sigma}_n(E, g, \alpha'(-t), E_N) = E_N^{D/2-1} \alpha'(-t)^{-D/2} \tilde{\sigma}_n\left(\frac{E}{E_N}, g, 1, 1\right) = E_N^{D/2-1} \alpha'^{-D/2} e^{-tzD/2} \tilde{\sigma}_n\left(\frac{E}{E_N}, g, 1, 1\right), \tag{4.52}$$

$$\Delta_n(g, \alpha'(-t), E_N) = E_N^{D/2-1} \alpha'(-t)^{-D/2} \Delta_n(g, 1, 1) = E_N^{D/2-1} \alpha'^{-D/2} e^{-tzD/2} \Delta_n(g, 1, 1). \tag{4.53}$$

So far, Eq. (4.51) together with (4.52) and (4.53) is valid for all values of t. We now consider what happens for small ξ ($t \to -\infty$). In this limit, we know that

$$U(-t) \sim U e^{rt}, \tag{4.50}$$

$$\int_{-t}^{0} dt'\, U(t')^n \sim U^n \frac{1}{nr} (e^{rtn} - 1). \tag{4.54}$$

So the U dependence on the right-hand side of Eq. (4.51) becomes fairly simple, and if we equate the coefficient of U^n on both sides, we find that

$$\tilde{\sigma}_{n+2}(\xi E, g, \alpha', E_N) \underset{\xi \to 0}{\sim} \exp[(2\gamma_1 - 1 + zD/2)t] \times \sum_{k=1}^{n+1} c_{nk}\, e^{rt(k-1)}, \tag{4.55}$$

where the constants c_{nk} are combinations of γ_{Nn}, $\tilde{\sigma}_n(E/E_N, g, 1)$, and $\Delta_n(g, 1, 1)$. Finally, putting $\omega = \xi E$, we have

$$\tilde{\sigma}_{n+2}(\omega, g, \alpha', E_N) \underset{\omega \to 0}{\sim} \omega^{2\gamma_1 - 1 + zD/2} \times \sum_{k=1}^{n+1} c_{nk}\, \omega^{r(k-1)}. \tag{4.56}$$

We can transform to rapidity and obtain

$$\sigma_{n+2}(Y) \sim \sigma_{el}(Y) U^n (\tilde{c}_{n1} + \tilde{c}_{n2} Y^{-r} + \cdots + \tilde{c}_{n\,n+1} Y^{-nr}). \tag{4.57}$$

This is the key result of the calculations of this section.

Before we turn to a discussion of this result, we would like to point out that the infrared behavior (4.55) of $\tilde{\sigma}_{n+2}$ strongly depends on how $U(t)$ approaches its fixed-point value. For example, if $\beta_U = cU^2 + O(U^3)$ has a double zero at $U=0$ (i.e., $r=0$), then $U(-t)$ has the form

$$U(-t) = \frac{U}{1 - Uct}, \tag{4.58}$$

and the analog to (4.56) would be

$$\tilde{\sigma}_{n+2}(\omega) \sim \omega^{2\gamma_1 - 1 + zD/2} (\ln \omega)^n. \tag{4.59}$$

This would have been, for example, the result in the absence of cuts at $D=2$.

B. Results and discussion

After these rather long calculations let us pause for a moment and contemplate what we have achieved. We first derived a scaling law for the partial-wave amplitude F_n (4.29) and the scattering amplitude $T_{2\to n}$ (4.30). If we use this result to evaluate the cross section σ_n, we obtain

$$\sigma_{n+2} \sim Y^{2\beta - (n+1)(2\beta + 2\gamma_1 + zD/2 - 1) - 1} \int \prod_{i=1}^{n+1} (dx_i d^D k_i) \delta(1 - \sum x_i) |T_{2\to n+2}(x_i, \vec{k}_i)|^2, \tag{4.60}$$

with $x_i = y_i/Y$. This is the result of Migdal, Polyakov, and Ter-Martirosyan.[1] However, we know that the x_i integration is divergent at $x_i = 0$, and, therefore, only if we restrict the x_i to be greater than some finite cutoff, say $x_i \geq a$ ($y_i \geq aY$), is the right-hand side of Eq. (4.60) defined. Any energy-dependent cutoff would introduce further energy dependence of the integral in (4.60), over which we have no control.

Since we anticipated this danger, we developed our RFT for the cross sections. The result for σ_n is written in (4.57):

$$\sigma_{n+2}(Y) \sim \sigma_{\rm el}(Y) U^n (\tilde{c}_{n1} + \tilde{c}_{n2} Y^{-r} + \cdots + \tilde{c}_{n\,n+1} Y^{-nr}) . \tag{4.57}$$

The most prominent feature of this is clearly that the asymptotic energy behavior of σ_n is the same as for $\sigma_{\rm el}$. We have kept the nonleading terms because they show the resemblance to our simple model in Sec. II (2.10). Let us take, for example, the last term in (4.57). It has just the same behavior as obtained in (4.60), because

$$Y^{2\beta-(n+1)(2\beta+2\gamma_1+\varepsilon D/2-1)} = Y^{1-2\gamma_1-\varepsilon D/2} Y^{-nr} , \tag{4.61}$$

and $Y^{1-2\gamma_1-\varepsilon D/2}$ is the asymptotic behavior of $\sigma_{\rm el}$. But we know that the power of Y in (4.60) belongs to that configuration of particle production where all rapidity gaps are large. We, therefore, identify the last term in (4.57) as the contribution of this region of phase space. As to the other terms in (4.57), we use the analogy to our model in Sec. II. Equation (4.57) is the expansion in the number of large rapidity gaps, and the leading contribution comes from the first term where only one rapidity gap is large. We illustrate this situation in Fig. 12. We plot the rapidity distribution of the produced particles of a single event. In the leading term of (4.57) [Fig. 12(a)], we have one "hole" (in order to preserve symmetry, this hole can be between any two of the outgoing particles), in the next term, two holes and so forth. In the last term, the produced particles are uniformly distributed [Fig. 12(c)].

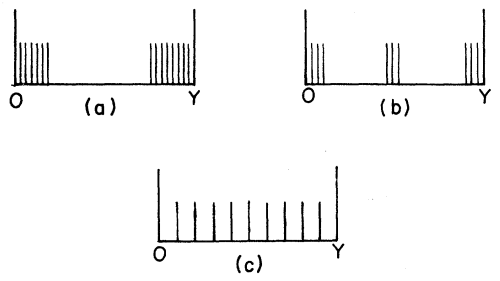

FIG. 12. Particle configurations in $\sigma_n(Y)$. (a) The leading contribution with one large gap, (b) the next-leading contribution with two large gaps, (c) the last contribution where the particles are distributed uniformly.

Looking at Fig. 12 we make another observation. It has been argued[23,24] that high-energy scattering in RFT with a Pomeron having intercept 1 can be viewed as a critical phenomenon. One of the characteristics of phase transitions is the simultaneous existence of different phases of the system. In hadron scattering, different phases correspond to different densities in rapidity of particle production. This feature is exhibited in Figs. 12(a) and 12(b), where rapidity regions with high particle density (particle clusters) are adjacent to regions with zero density (holes). This situation has to be confronted with Fig. 12(c), which represents the last (nonleading) contribution in (4.57): This type of particle production is what one would expect in the usual multiperipheral models.

In all these considerations, the picture obtained from our simple model of Sec. II has served as a rather faithful guide. In fact, comparing the multi-Pomeron exchange without cuts in $D > 2$ transverse dimensions with our RFT result we find that the qualitative picture has not changed. In both cases we have $\sigma_n \sim \sigma_{\rm el}$. [A consequence of this is that those types of production which are present only when cuts are included, e.g., Fig. 4(c), leave no signature on $\sigma_n(Y)$.] Only at $D = 2$ does the presence of cuts lead to a change. Without cuts, we have from (2.8)

$$\sigma_n(Y) \sim \frac{(\ln Y)^{n-2}}{Y} , \tag{2.8}$$

and in this contribution all rapidity gaps are large. Once the triple-Pomeron coupling is turned on, we have (4.57), and the produced particles prefer a very different configuration.

Our result (4.57) can further be illustrated by a simple counting rule of anomalous dimensions. If we think of a production process where only *one* renormalized Pomeron is exchanged between two renormalized $\tilde{P}P\tilde{P}$ vertices, then a simple counting of anomalous dimensions coming from the Pomeron propagators (4.14) and the $\tilde{P}P\tilde{P}$ vertices (4.25) leads to

$$\sigma_n(Y) \sim \text{const} \times \int \prod_{i=1}^{n-1} dy_i \delta(Y - \textstyle\sum y_i) \frac{1}{y_i^{1+r}} , \tag{4.62}$$

with r given in (4.48). Repeating the arguments given in Sec. II, this leads to (4.57) and may serve as a heuristic way of tracing the effect of anomalous dimensions.

In these calculations we have not included nonenhanced graphs which, once finite values of rapidities appear, are no longer negligible. How-

ever, the fact that for large s all (but one) rapidity gaps are pushed down to their lower limit is dictated by the enhanced graphs. In other words, if we would include nonenhanced graphs in our calculations, then the infrared behavior of $U(t)$ and, hence, the asymptotic expansion of $\sigma_n(Y)$ in (4.57) would not be affected. This, again, is a consequence of the results of Bardeen *et al.*[22]

This completes our treatment of the asymptotic behavior of the fixed-multiplicity cross sections. The next problem to be addressed is the high-energy behavior of $\sigma(Y)$, the sum of $\sigma_n(Y)$. One might be tempted to derive this from the infrared behavior of $\sigma(E)$ in (4.46). If we use for σ and Δ on the right-hand side of (4.46) the scaling argument (4.52) together with the infrared freedom of $U(-t)$, we obtain

$$\sigma(\xi E, g, \alpha', U, E) \sim \xi^{2\gamma_1 - 1 + zD/2}, \tag{4.63}$$

or

$$\sigma(Y) \sim \sigma_{el}(Y). \tag{4.64}$$

This obviously represents the sum of the leading terms of $\sigma_n(Y)$ in (4.57):

$$\sigma(Y) = \sigma_{el} \sim \sum_n U^{n-2}(\tilde{c}_{n1} + \cdots + \tilde{c}_{nn+1} Y^{-nr}). \tag{4.65}$$

But here again the experience from Sec. II provides us with a warning. For small U, the sum of leading terms converges and might yield the correct behavior of $\sigma(Y)$, but when U becomes larger, the sum of leading terms begins to diverge, and the neglect of the nonleading terms is certainly no longer justified. What in fact may happen is that a new power of s is built up, which may violate the Froissart bound. Such a situation would correspond to a new singularity of $\sigma(E)$ in the E plane. To find the correct behavior of $\sigma(Y)$, we therefore turn to a study of possible new singularities of $\sigma(E)$ away from $E = 0$.

V. FINKELSTEIN-KAJANTIE PROBLEM IN RFT

The question whether repeated Pomeron exchange leads to a new singularity of $\sigma = \sum \sigma_n$ to the right of $j = 1$ and, hence, leads to violation of the Froissart bound is actually one of the main interests in studying these production processes. Originally, Finkelstein and Kajantie[11] demonstrated that along a specific line in the $(n, \ln s)$ plane $\sigma_n(s)$ grows faster than allowed by unitarity. But this is just the reflection of a new singularity in $\sigma(E)$ to the right of $j > 1$. In Sec. II we mentioned that when $p = 0$ the existence of such a singularity is unavoidable, no matter how small we make the $\tilde{P}P\tilde{P}$ coupling. For $p > 0$, on the other hand, a small-enough U might prevent the existence of a singularity above 1. In the last section we learned that RFT resembles very closely the simple model of Sec. II with $p = D/2 - 1 > 0$. So our expectation is that in our model for small U we have no new singularity, while for large U we may still have problems.

We will now demonstrate that this expectation is correct. The search for a new singularity which corresponds to a two-Pomeron bound state requires, in principle, more than just studying infrared properties of the Green's function, and it seems as if the tools of the RGE used in the previous sections are not adequate. However, the knowledge of the β_U function provides us with enough information to ensure that the singularity which causes the Finkelstein-Kajantie problem in the simple pole model, disappears once cuts are included. Before we start any calculations, let us sketch the main idea, following Gross and Neveu.[25] Let us consider the (renormalized) 2 Pomeron $\to$ 2 Pomeron Green's function $\Gamma^{22}(E_i, \vec{k}_i, U, E_N)$, where we have suppressed the dependence on all other parameters. At a renormalization point it defines the quartic coupling U:

$$U = \Gamma^{22}(E_i, \vec{k}_i, U, E_N)\Big|_{\substack{E_i = -E_N/2 \\ \vec{k}_i = 0}}, \tag{5.1}$$

On the other hand, we have a RGE:

$$(\xi \partial_\xi - \beta_U \partial_U)\Gamma^{22}(\xi E_i, \vec{k}_i, U, E_N) = 0, \tag{5.2}$$

with the solution

$$\Gamma^{22}(\xi E_i, \vec{k}_i, U, E_N) = \Gamma^{22}(E_i, \vec{k}_i, U(-t), E_N). \tag{5.3}$$

Choosing in (5.3) $E_i = -E_N/2$, $\vec{k}_i = 0$, we have on the right-hand side by the definition (5.1)

$$\Gamma^{22}(\xi E_i, \vec{k}_i, U, E_N) = U(-t). \tag{5.4}$$

Now the function $U(t)$ is, as usual, defined by

$$\frac{dU(t)}{dt} = -\beta_U(U), \quad U(0) = U. \tag{5.5}$$

This equation is solved by

$$t = -\int_U^{U(t)} \frac{dx}{\beta_U(x)}. \tag{5.6}$$

Now suppose that $\beta_U(x) < 0$ for all $x > U$, and the integral

$$T = -\int_U^\infty \frac{dx}{\beta_U(x)} < \infty \tag{5.7}$$

converges at infinity. Then it follows from (5.6) that $U(t)$ has an infinity at $t = T$. But because of

(5.4), $U(T)=\infty$ implies also

$$\Gamma^{22}(-e^{T}E_N/2, 0, U, E_N)=\infty . \tag{5.8}$$

This shows how a singularity in Γ^{22} can be traced in the behavior of β_U. In the following we will use this method, in order to compare the question of new singularities in the Finkelstein-Kajantie case with our RFT model.

Let us first examine the β_U function in the absence of triple-Pomeron interactions. Then only the graphs of Fig. 5 contribute to $\sigma(E)$, and Γ^{22} is given by

$$\Gamma^{22}(E_i, \vec{k}_i, \alpha', U_{d0})_{\text{unren}} = \Gamma^{22}(E_i, \vec{k}_i, \alpha', U_d)_{\text{ren}}$$

$$= \frac{U_{d0}}{1-U_{d0}[\frac{1}{2}\alpha'(\vec{k}_1+\vec{k}_2)^2-E_1-E_2]^{D/2-1}\alpha'^{-D/2}\Gamma(1-\frac{1}{2}D)(\frac{1}{2}\pi)^{D/2}} \tag{5.9}$$

and, following (5.1),

$$U_d=\frac{U_{d0}}{1-U_{d0}E_N{}^{D/2-1}\alpha'^{-D/2}\Gamma(1-\frac{1}{2}D)(\frac{1}{2}\pi)^{D/2}} . \tag{5.10}$$

In (5.9) and (5.10), we have given U a subscript d in order to indicate that U still has dimensions. Using the dimensionless combination

$$U=\frac{U_d E_N{}^{D/2-1}}{\alpha'^{D/2}}, \tag{5.11}$$

we obtain for the β_U function the exact form

$$\beta_U=\left(\frac{D}{2}-1\right)U-U^2K, \tag{5.12}$$

where

$$K=\Gamma\left(2-\frac{D}{2}\right)\left(\frac{\pi}{2}\right)^{D/2} . \tag{5.13}$$

We have plotted the behavior of β_U in (5.12) in Fig. 13 for both $2<D<4$ and $D=2$. Using the arguments given above we note the following:

(a) $2<D<4$. β_U has two zeros at $U=0$ and $U_c>0$, the point $U=0$ being infrared stable. If the physical value U is chosen to be in the range $[0, U_c]$, the effective U will be driven to zero. For the physical $U>U_c$, the effective U moves to the right, and according to our argument above, there exists a value T for t such that $U(T)=\infty$, and a singularity at $E<0$ or $j>1$ exists. All this can be made explicit by solving Eq. (5.5):

$$U(t)=\frac{D/2-1}{K}\frac{e^{-(D/2-1)t}}{(D/2-1)/KU-1+e^{-(D/2-1)t}}, \tag{5.14}$$

and choosing for U values within $[0, U_c]$ or $U>U_c$, respectively $[U_c=(D/2-1)/K]$. [A closer look at (5.14) with $0<U<U_c$ tells us that even in this case a pole exists, if we allow for complex values of t. However, one can show that this corresponds to a singularity of Γ^{22} on an unphysical sheet of the E plane, as long as $2<D<4$, and, therefore, it is of no interest for us.]

(b) $D=2$. We start with case (a) and let D approach 2. Since the value of $U_c=(D/2-1)/K$ goes to zero, the interval $[0, U_c]$ shrinks to zero, and at $D=2$ there are no values for U left where $U(t)$ would not encounter a pole. Solving again (5.5)

$$U(-t)=\frac{U}{1+KUt}, \tag{5.15}$$

we see that for any value U a pole occurs at

$$t=-\frac{1}{KU} \text{ or } \xi=e^{t}=e^{-1/KU} . \tag{5.16}$$

Since $E=1-j=-\xi E_N/2$, this singularity lies to the right of $j=1$:

$$j=1+\xi\frac{E_N}{2}$$

$$=1+\frac{E_N}{2}e^{-1/KU} . \tag{5.17}$$

[It is important to note that, as a consequence of our method of regularizing divergent integrals, Eqs. (5.10) and (5.17) describe the physical situation reliably only for $|E|\lesssim E_N$. But this is all we need for our purpose.] The results from (a) and (b) agree exactly with what we had anticipated in Sec. II.

Now we want to see to what extent the situation changes when a triple-Pomeron coupling is present. In the last section we discovered a close similarity between our RFT model and the Finkelstein-Kajantie case for $2<D<4$ transverse dimen-

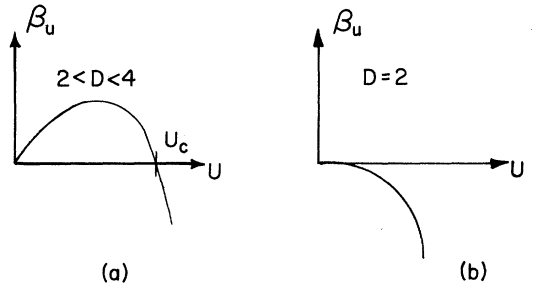

FIG. 13. The β_U function in the absence of Pomeron cuts (a) for $2<D<4$, (b) for $D=2$.

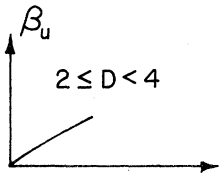

FIG. 14. The β_U function when cuts are included ($2 \leq D < 4$).

sion. This leads us to the expectation that the situation of our RFT model will be similar to case (a) above. That this is correct follows from β_U (Fig. 14) which we studied in the last section. We found that the slope of β_U at $U=0$ is positive and different from zero, for $2<D<4$ as well as $D=2$. This, together with our argument given above, guarantees that there exists a range of values U such that the effective coupling constant $U(t)$ is driven to zero without encountering a singularity. For the physical U being within this range, no new singularity is generated, and violation of s-channel unitarity is avoided. *This proves that in our RFT the Finkelstein-Kajantie problem no longer exists.*

Having ensured the existence of a range of U values, for which unitarity is obeyed, one still may ask what happens if U becomes large. Before we try to find an answer to that question, we first introduce a slight modification into our theory which will not affect any of our previous results on $\sigma_n(Y)$ but will allow us to continue our theory to $D=4$ dimensions. As we said in the previous section, the RFT given by the Lagrangian (3.10) is not renormalizable at $D=4$, although the infrared behavior of $\sigma(E)$ and $\sigma_n(E)$ remains valid at $D=4$. But now we want to know a little bit more than only the infrared behavior of $U(t)$ and would like to determine the β function at least to order U^2. The difficulty with our theory at $D=4$ becomes already visible in the absence of Pomeron cuts: The U^2 term in the β_U function in (5.12) is not defined at $D=4$, since K (5.13) becomes infinite. We can avoid this by including another term in the bare Pomeron trajectory and propagator[26]

$$\alpha_p(t) = 1 + \alpha_0' t + a_0 \alpha_0' t^2 . \tag{5.18}$$

This changes $\mathfrak{L}_{0i}$ in (3.10),

$$\mathfrak{L}_{0i} \to \tfrac{1}{2} i \psi_i^\dagger \overleftrightarrow{\partial}_t \psi_i - \alpha_0' \nabla \psi_i^\dagger \cdot \nabla \psi_i - a_0 \alpha_0' \nabla^2 \psi_i^\dagger \nabla^2 \psi_i - \Delta_0 \psi_i^\dagger \psi_i , \tag{5.19}$$

and makes the theory renormalizable at $D=4$. When applied to the Finkelstein-Kajantie case, this theory reproduces the correct results for the whole interval $2 \leq D \leq 4$. In the presence of a triple-Pomeron coupling it has been shown[26] that the t^2 term in (5.18) does not affect the infrared behavior of g and α', and thus, had we included this term into our previous calculations, none of our conclusions would have changed.

Now our theory with (5.19) for $\mathfrak{L}_{0i}$ in (3.10) is renormalizable at $D=4$, and we start considering β_U at D near 4. Because of the presence of the triple-Pomeron coupling, it is now no longer possible to compute the exact β_U function. However, we know that for $\epsilon = 4 - D$ small, the effective triple-Pomeron coupling is small, and β_U will not too much differ from the case without a triple-Pomeron vertex. In the Appendix we show this in some detail. Then the situation can be described by the β function of Fig. 13(a): There is a range $[0, U_c]$ for which the effective coupling constant U is driven to zero, and no singularity occurs. For $U > U_c$, a singularity appears. We conclude from this that in the neighborhood of $D=4$, our RFT model contains still a new singularity when U is large enough.

If we go away from $D=4$, we loose the control over the large-U behavior of β_U. All we know is that the slope r of β_U of $U=0$ remains positive and nonzero all the way down to $D=2$, which proves the absence of a singularity as long as U is small enough. Whether the singularity associated with large U survives cannot be decided.

Before we turn to a discussion we have to add one missing link to our argument. The argument that we have made about the existence or nonexistence of a singularity applies to the 2 Pomeron $\to$ 2 Pomeron Green's function Γ^{22}, and we have to make sure that in going from Γ^{22} to $\sigma(E)$ the situation remains unchanged. It is clear that if Γ^{22} has no singularity $\sigma(E)$ will have none either. On the other hand, if Γ^{22} becomes infinite for some value of its external energies and momenta, this singularity will not be washed out by going from Γ^{22} to $\sigma(E)$. One verifies this by taking a look at Eq. (4.46) which expresses $\sigma(E)$ in terms of the effective coupling $U(t)$. The singularity of Γ^{22} was found to arise when $U(t)$ becomes infinite. In (4.46), an infinity in $U(t)$ will, in general, also lead to a singularity of $\gamma_N(g(t), U(t))$ and, hence to a singularity of $\sigma(E)$.

Let us now discuss some implications of our results. First we notice that our RFT model has again the same qualitative features as our simple model with $p = D/2 - 1 > 0$ of Sec. II. It is only the point $D=2$ where the simple pole model becomes very peculiar, while RFT retains the same behavior that it had for $2<D<4$. The nice consequence of this is that RFT at $D=2$ obeys the Froissart bound, provided we take the $\tilde{P}P\tilde{P}$ vertex (the quartic coupling U is the square of the $\tilde{P}P\tilde{P}$ vertex) not too large. This taken to be the

case, the asymptotic behavior of $\sigma(Y)$ is given by the infrared behavior of $\sigma(E)$, namely, (4.63), (4.64):

$$\sigma(Y) \sim \sigma_{el}(Y). \tag{5.20}$$

Since in RFT it turns out in all performed approximations[1,2,3,19,20] that $\sigma_{el}(Y) < \sigma_{tot}(Y)$, there is no problem with unitarity.

The result (5.20) has an important consequence for the formation of the total cross section. Since $\sigma(Y)$ is smaller than σ_{tot}, the production process with repeated Pomeron exchange is not the most relevant contribution to σ_{tot}. This is different from certain absorptive models[5] where the Pomeron can consistently be built up by processes involving only Pomeron exchange. The fact that in our model Pomeron-dominated production processes are not sufficient to build σ_{tot} leads us to consider processes with secondary Regge poles, and we will do this in Sec. VII.

The next comment we want to make concerns the consequences of our result for other RFT models. We have stressed the importance of nonzero anomalour dimensions, resulting from the Pomeron self-interaction. This leads to the expectation that in infrared-free RFT's (weak-coupling Pomeron), where such anomalous dimensions do not appear, s-channel unitarity will be violated. In fact, more detailed calculations for the ϕ^4 Pomeron theory (which is described in Ref. 21) show that the Finkelstein-Kajantie problem is not solved, and a singularity above 1 is generated for all values of $\tilde{P}P\tilde{P}$ coupling. This points out to difficulties exhibited in infrared-free RFT's.

Finally, we want to say a few words about the possibility that in our model, if the $\tilde{P}P\tilde{P}$ vertex is large enough, we still may have a singularity above $j=1$. We found that it exists near $D=4$ transverse dimensions and may very well survive when going to $D=2$. If this is the case, then we either have to conclude that unitarity restricts the range of allowed values of the $\tilde{P}P\tilde{P}$ vertex, or we have to search for other inelastic processes that might help to eliminate the singularity. Clearly, the production processes that we have considered are not complete in the sense of s-channel unitarity. Namely, if we decompose the Reggeon diagram in Fig. 15(a) into diagrams of the sort discussed by Abramovskiĭ, Gribov, and Kancheli,[27] then we obtain, in addition to our contribution [Fig. 15(b)], also the configuration Fig. 15(c) which stands for other types of multiparticle production. From this point of view it may be that singling out the production process of the Finkelstein-Kajantie type is just an unfortunate way of cutting the total cross section into pieces. These, however, are speculations, and calculations have to be done, before one can rely upon this. For the moment we will be content with having a range of values for the $\tilde{P}P\tilde{P}$ vertex where there is no need to search for cancellation mechanisms.

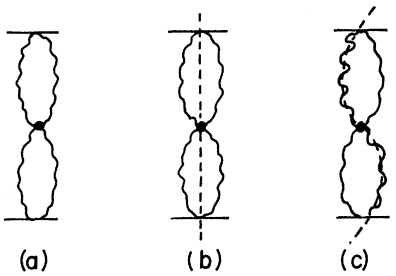

FIG. 15. Different cuttings of a contribution to σ_{tot}.

VI. POMERON-PARTICLE-REGGEON VERTEX

In order to complete our plan, we have to show that the way in which s-channel unitarity is restored does not lead to any decoupling problems. We have seen that in our model the basic mechanism which reconciles the repeated Pomeron exchange with s-channel unitarity is the screening of the $\tilde{P}P\tilde{P}$ vertex (4.25). This scaling law tells us that, when both Pomeron energies and momenta go to zero, the vertex vanishes. The form (4.25) of the $\tilde{P}P\tilde{P}$ vertex has to be compared with another form which has been suggested to restore s-channel unitarity in production processes:

$$\Gamma_{\tilde{P}P\tilde{P}}(t_1, t_2) = (t_1 + t_2)[a + O(t_1, t_2)]\,. \tag{6.1}$$

The basic difference between this and (4.25) is that in (4.25) the $\tilde{P}P\tilde{P}$ vertex depends also on the two adjacent angular momenta. This dependence leads, via the Sommerfeld-Watson transform, to inverse powers of $\ln s$, and it is these powers which prevent the cross sections from rising too strongly.

The form (6.1) is known[7] to lead to the decoupling theorems. (In the literature, decoupling theorems are usually derived from inclusive sum rules.[28] But it is possible to arrive at the same conclusions in the framework of multiparticle production processes.) Because of the difference between (6.1) and (4.25), RFT has a good chance to avoid these difficulties. For a more detailed examination of this point, we repeat the argument which, when applied to (6.1), leads to the decoupling problems.

Instead of considering the production of n single particles via Pomeron exchange we now take the productions of n particle pairs, and assume their invariant mass to be sufficiently large. Then, for an appropriate choice of quantum numbers,

FIG. 16. Opening of the $\tilde{P}$-(2-particle)-$\tilde{P}$ vertex. The horizontal straight line denotes the Regge pole.

FIG. 18. A diagram that does not contribute to the Regge pole.

a secondary Regge pole with mass t_R is exposed between the two particles (Fig. 16). We now consider the cross sections σ_n for the production of n such pairs with fixed invariant mass M^2 and fixed internal momentum transfer $t_R \neq 0$. Without any cut corrections and using a nonvanishing $\tilde{P}PR$ vertex, we clearly violate s-channel unitarity in the same way as in the Finkelstein-Kajantie case. We, therefore, have to show that the Pomeron cuts are sufficient to avoid this disaster.

In order to be consistent we start with all possible enhanced diagrams (Fig. 17). We then isolate those which contribute to the Regge pole inside the particle pair (for example, the diagram in Fig. 18 has no Regge pole, but only a Regge-Pomeron cut, and this singularity is, for $t_R \neq 0$, well separated from the Regge pole), and examine whether they (Fig. 19) alone already satisfy s-channel unitarity. At first sight this seems to be a fairly strong demand, but a brief reflection shows that it is the simplest way to avoid complications. Namely, if these contributions were not enough to obey unitarity, we would have to add those diagrams that give rise to the $R\tilde{P}$ cut, $R\tilde{P}\tilde{P}$ cut, etc. and show that their sum respects unitarity. But if we take the Sommerfeld-Watson transform of the Reggeon energy, we obtain a Regge-pole contribution, a $R\tilde{P}$ cut, etc., and since the position of these singularities has different t_R dependences, these terms appear to be linearly independent from each other. It is, therefore, hard to imagine how a cancellation between all these terms might occur.

Returning to the $\tilde{P}PR$ vertex, we are prepared to find a screening, and this screening has to be strong enough. Before we start calculations, we point out that such a screening will not imply decoupling problems. Although we do not exactly know how to continue our RFT from negative t_R to positive values (on the way to $t_R > 0$ some approximations made in RFT are no longer valid, and new j-plane singularities emerge[29]), the Reggeon calculus of Ref. 12 tells us that *at the particle pole* ($t_R = m^2$, and physical angular momentum in the Reggeon channel) *all Pomeron-cut contributions must decouple,* and only the bare $\tilde{P}PR$ vertex survives which we take to be different from zero. The decoupling of all cut contributions at physical angular momentum is part of the Reggeon calculus for the production amplitude.[12]

We are now going to show that our RFT model does exactly what we expect, namely, the $\tilde{P}PR$ vertex is screened for $t_R \neq 0$, and the screening is strong enough. From a formal point of view, the existence of this screening is by no means obvious. For all scaling laws which have been derived in RFT are valid in the limit where *all* external Reggeon energies and momenta are scaled to zero. In our case, however, we consider the $\tilde{P}PR$ vertex at the point where the Reggeon, being on or close to its mass shell, stays away from zero ($t_R \neq 0$), and only the Pomeron is infrared.

To see why, nevertheless, an anomalous dimension is built up, we recall that the origin of an infrared anomalous dimension is the accumulation of infrared divergences. We, therefore, start by considering infrared singularities of some simple diagrams that contribute to the $\tilde{P}PR$ vertex. We take the Reggeon mass t_R to be negative and nonzero, and examine the limit of vanishing Pomeron variables ($E_1 \to 0$, $\vec{k}_1 \to 0$). We will find that in this limit an accumulation of infrared divergences occurs, and that we can separate certain diagrams which yield the most singular contribution (Fig. 20).

The simplest diagram is shown in Fig. 21(a) and consists of a single (ω, k) loop integration. A singularity of this integral occurs if two (or more) singularities of the integrand pinch the

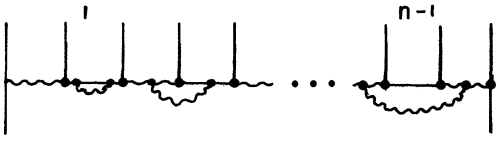

FIG. 17. Enhanced diagrams for the process $2 \to 2 + (n-1)$ particle pairs.

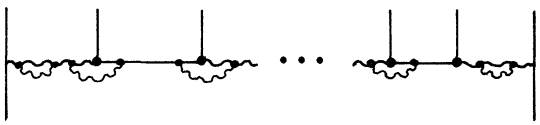

FIG. 19. A diagram that contributes to the Regge poles in all particle pairs.

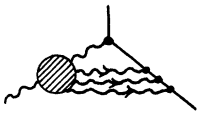

FIG. 20. Diagrams which contribute to the leading infrared behavior of the $\tilde{P}PR$ vertex.

integration contour, and using the standard techniques of Ref. 30, we find two infrared singularities. The one is the two-Pomeron cut and arises when the poles of the two Pomeron propagators pinch, the other is generated by the simultaneous singularities of all three propagators and occurs only if the Reggeon sits on its mass shell, i.e.,

$$E_2 = 1 - \alpha_R(k_2^2). \tag{6.2}$$

For both these singularities the relevant region of integration is that of small ω and $\vec{k}$, i.e., both Pomerons are infrared, and the internal Reggeon is close to its mass shell. A similar result holds for the diagram of Fig. 21(b): The most singular behavior is obtained when (6.2) is fulfilled, and in order to make the integral singular, all internal Pomerons have to be infrared and the internal Reggeons close to the mass shell.

In Fig. 21(c), we have no more infrared singularities than in Fig. 21(a), because the $\vec{k}_2$ loop produces no new singularity at $E_1 = 0$, $\vec{k}_1 = 0$. Thus, it has the same infrared behavior as Fig. 21(a) and only leads to (finite) renormalization of the $R\tilde{P}R$ vertex in Fig. 21(a). In the same way, a self-energy correction along the Reggeon line [Fig. 21(d)] only produces, when compared to Fig. 21(a), a new singularity in $E_2, \vec{k}_2$ (the Reggeon-Pomeron cut), which is well separated from the Regge pole. It yields no new contribution to the infrared limit $E_1 \to 0$, $\vec{k}_1 \to 0$. These two examples show that a Pomeron, omitted from the Reggeon line, does not enhance the infrared singularities and the most singular diagrams are those of Fig. 20.

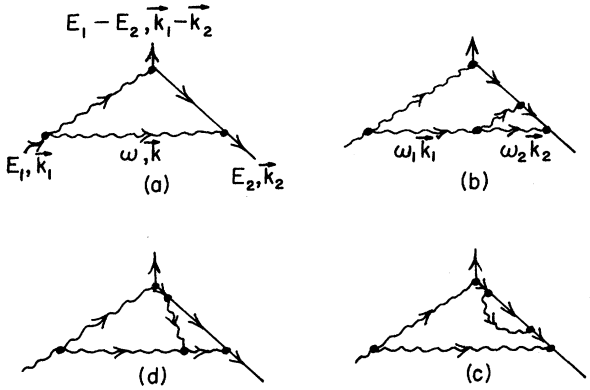

FIG. 21. Some lowest-order diagrams for the $\tilde{P}PR$ vertex.

We are now going to describe a theory that takes into account all diagrams of Fig. 20 and, to leading order, will give the correct infrared behavior of the $\tilde{P}PR$ vertex. We expand the Regge trajectory around its value at $t_R = -Q^2$:

$$\begin{aligned}\alpha_R((Q+k)^2) &= \alpha_R(Q^2) + \beta'[(Q+k)^2 - Q^2] \\ &= \alpha_R(Q^2) + 2\beta'\,\vec{Q}\circ\vec{k} + \beta' k^2,\end{aligned} \tag{6.3}$$

and drop the term $\beta' k^2$, because only small values of $\vec{k}$ are important for the infrared behavior. Our Reggeon propagator thus becomes

$$\begin{aligned}G_R &= i\{E - [\alpha_R(Q^2) - 1] - 2\beta'\,\vec{Q}\cdot\vec{k} + i\epsilon\}^{-1} \\ &= i\,(E - \Omega - 2\beta'\,\vec{Q}\cdot\vec{k} + i\epsilon)^{-1}.\end{aligned} \tag{6.4}$$

For the Pomeron we use the same propagator and self-interaction as before. Interaction between Pomeron and Reggeon takes place via a Pomeron + Reggeon → Reggeon vertex function, approximated by its value at zero Pomeron momentum and Q^2 Reggeon momentum. The Reggeon calculus of Ref. 12 tells us that this coupling is again purely imaginary. The Lagrangian for this theory is (Fig. 19)

$$\mathcal{L} = \mathcal{L}_0 - \frac{i g_0}{2}\psi^\dagger\psi(\psi + \psi^\dagger) + \frac{i}{2}\phi^\dagger\overleftrightarrow{\partial}_t\phi - [1 - \alpha_R(Q^2)]\,\phi^\dagger\phi - [2\beta'\phi^\dagger\,\vec{Q}\cdot\nabla\phi + \text{H.c.}] - i W_0\psi^\dagger\phi^\dagger\phi, \tag{6.5}$$

where $\mathcal{L}_0$ [given in (3.4)] is the free Pomeron part, ψ and ϕ are field operators for Pomeron and Reggeon, respectively. The $\tilde{P}PR$ vertex is, as before, given by a source term $V_0\psi^\dagger\phi$. For the term $[1 - \alpha_R(Q^2)]\,\phi^\dagger\phi$ we use the idea of Abarbanel and Sugar[31] and shift the Reggeon energy by replacing $\phi \to \exp\{it[1 - \alpha_R(Q^2)]\}\phi$. As a result of this, the "intercept" of our Reggeon is zero rather than Ω.

For the examination of the infrared behavior of the $\tilde{P}PR$ vertex we proceed in the same way as we did before with the $\tilde{P}P\tilde{P}$ vertex, i.e., we define renormalized quantities and write down the RGE. In doing this we observe that the renormalization of the Pomeron quantities (field renormalization, slope, and triple-Pomeron coupling) is independent of the interaction with the Reggeon. Furthermore, the Reggeon field and slope β' remain unchanged through renormalization, because we have dropped the Pomeron

FIG. 22. Lowest-order renormalization of the $\tilde{P}PR$ vertex.

emission from the Reggeon ($\psi\phi^\dagger\phi$ interaction). The only new renormalization conditions are, therefore, those for the $\tilde{P}PR$ vertex (i.e., the $V_0\psi^\dagger\phi$ source term), the $\tilde{P}RR$ vertex and the renormalized coupling W:

$$\Gamma_{\tilde{P}RR} = Z_1^{1/2}\Gamma_{\tilde{P}RR;\,\mathrm{unren}}, \tag{6.6}$$

$$\Gamma_{\tilde{P}PR} = Z_5^{-1}Z_1^{1/2}\Gamma_{\tilde{P}PR;\,\mathrm{unren}}, \tag{6.7}$$

$$\Gamma_{\tilde{P}PR}(E_1,E_2,\vec{k}_1,\vec{k}_2)\Big|_{\substack{E_1=E_2=-E_N=\\ \vec{k}_1=\vec{k}_2=0}} = \frac{W_d}{(2\pi)^{D+1}}, \tag{6.8}$$

$$\Gamma_{\tilde{P}PR}(E_1,E_2,\vec{k}_1,\vec{k}_2)\Big|_{\substack{E_1=E_2=-E_N\\ \vec{k}_1=\vec{k}_2=0}} = 1. \tag{6.9}$$

In (6.8) and (6.9), we have suppressed the dependence on the parameters of our theory (α', g, β', W) and on the renormalization point. W_d on the right-hand side of (6.8) still has dimensions. We define

$$\mu = (-Q^2)^{1/2}\frac{\beta}{(\alpha' E_N)^{1/2}}, \tag{6.10}$$

$$W = W_d E_N^{\,D/4-1}\alpha'^{\,-D/4}\mu^{-1} = W_d E_N^{\,(D/2-1)/2}\alpha'^{\,(1-D/2)/2}\beta^{-1}. \tag{6.11}$$

The RGE for $\Gamma_{\tilde{P}PR}$ is

$$\left[\xi\frac{\partial}{\partial\xi} - \beta_g\partial_g - (\zeta-\alpha')\partial_{\alpha'} - \beta_W\partial_W - \beta_\mu\partial_\mu - (\gamma_5 - \tfrac{1}{2}\gamma_1)\right] \times \Gamma_{\tilde{P}PR}(\xi E_i, \vec{k}_i) = 0, \tag{6.12}$$

with

$$\beta_W = E_N\partial_{E_N}W, \tag{6.13}$$

$$\beta_\mu = E_N\partial_{E_N}\mu = -\tfrac{1}{2}(\zeta/\alpha' + \tfrac{1}{2}), \tag{6.14}$$

$$\gamma_5 = E_N\partial_{E_N}\ln Z_5, \tag{6.15}$$

and the other quantities as defined earlier. For β_W we calculate the lowest-order contribution to $\Gamma_{\tilde{P}RR}$ (Fig. 22) and obtain

$$\beta_W = \left[\left(\frac{D}{4}-\frac{1}{2}\right)\left(1-\frac{\zeta}{\alpha'}\right)+\frac{1}{2}\gamma_1\right]W + \frac{gW}{(2\pi)^D}\pi^{D/2}\Gamma\left(3-\frac{D}{2}\right)\mu\int_0^1 dx(1+x)^{-D/2}\left(1-\frac{x}{2}\right)\left[1-\frac{x}{2}+\frac{(1-x)^2}{(1+x)}\mu^2\right]^{D/2-3}, \tag{6.16}$$

which at $D=2$ implies the existence of an infrared-stable fixed point $\bar{W}\neq 0$. But rather than evaluating its numerical value in this approximation, we make the following observation. Looking at the graphs that contribute to the renormalization of $\Gamma_{\tilde{P}PR}$ and $\Gamma_{\tilde{P}RR}$, and using our renormalization conditions (6.8), (6.9), we have

$$W_d = W_{d0}Z_1^{1/2}\Gamma_{\tilde{P}PR;\mathrm{unren}}\big|_{\text{ren point}}, \tag{6.17}$$

$$Z_5 = Z_1^{1/2}\Gamma_{\tilde{P}PR;\,\mathrm{unren}}\big|_{\text{ren point}}, \tag{6.18}$$

and

$$\beta_W = \left[\left(\frac{D}{4}-\frac{1}{2}\right)\left(1-\frac{\zeta}{\alpha'}\right)\right]W + \beta'\alpha'^{\,1/2-D/4}E_N^{\,D/4-1/2}E_N\partial_{E_N}(W_{d0}Z_1^{1/2}\Gamma_{\mathrm{unren}}), \tag{6.19}$$

$$\gamma_5 = Z_5^{-1}E_N\partial_{E_N}(Z_1^{1/2}\Gamma_{\mathrm{unren}}). \tag{6.20}$$

At $D=2$, a zero of β_W implies $\gamma_5=0$, and the solution to the RGE is

$$\Gamma_{\tilde{P}PR}(\xi E_1,\xi E_2,\vec{k}_1,\vec{k}_2,\alpha',g,W,\mu,E_N) \sim \xi^{-\gamma_1/2}\Gamma_{\tilde{P}PR}(E_1,E_2,\vec{k}_1,\vec{k}_2,\alpha'(-t),\mu(-t),g(-t),W(-t),E_N). \tag{6.21}$$

Taking E_2 and $\vec{k}_2$ to zero (i.e., the Reggeon on its energy-momentum shell) and making use of the fact that $\Gamma_{\tilde{P}PR}$ is dimensionless, we rewrite

$$\Gamma_{\tilde{P}PR}(\xi E_1,0;\xi^{\varepsilon/2}\vec{k}_1,\alpha',g,W,\mu,E_N) \sim \xi^{-\gamma_1/2}\phi\left(\frac{E_1}{E_N},\frac{\alpha'\vec{k}_1^{\,2}}{E_N},\bar{g},\bar{W},\mu(-t)E_N\right). \tag{6.22}$$

The scaling function ϕ approaches a finite limit as $\mu\to\infty$.

It is now straightforward to see that the screening in (6.22) is strong enough to prevent the cross sections σ_n for the production of n pairs with fixed but large invariant mass and fixed internal momentum transfer $t_R\neq 0$ from violating s-channel unitarity. From (6.22) it follows that the $\tilde{P}$-particle-pair-$\tilde{P}$ vertex has the anomalous dimensions $-\gamma_1$, and this has to be compared with the dimension β for the $\tilde{P}P\tilde{P}$ vertex. From the discussion of the last two sections we know that

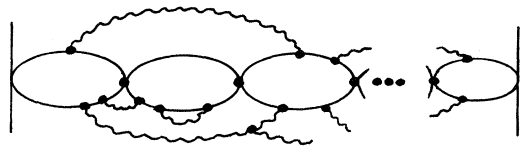

FIG. 23. Reggeon diagrams for multiparticle production via secondary Reggeon exchange.

the quantity which ensured the restoration of s-channel unitarity was [cf. (4.47)]

$$r = 2\gamma_1 + 2\beta + \tfrac{1}{2} Dz - 1.$$

Taking for β what is now the screening exponent of the $\tilde{P}$–particle-pair–Pomeron vertex, namely, $-\gamma_1$, we find that $r = z\,D/2 - 1$ is still positive, and all our discussions in the preceding sections tell us that there is no violation of s-channel unitarity. *This completes our demonstration that repeated Pomeron exchange in RFT respects s-channel unitarity without decoupling problems.*

VII. OTHER PRODUCTION PROCESSES

The study of production processes presented in the former section was mainly centered around consistency questions. We showed that repeated Pomeron exchange in multiparticle production processes no longer violates s-channel unitarity constraints once absorption is included and the $\tilde{P}P\tilde{P}$ coupling is not too large. However, the very way by which the Froissart bound is restored, namely, the screening of the production vertices, led also to the result that the part of the total cross section which is built up by those processes is proportional to σ_{el}. The ratio of σ_{el} to σ_{tot} is, whichever of the available numerical values for the critical indices one takes, a decreasing function of s, and processes with repeated Pomeron exchange are thus not the main part of σ_{tot}. This leads to the question which multiparticle production processes do build up the increasing cross section.

The candidate for generating the Pomeron singularity are production processes mediated by non-Pomeron exchange. However, we have seen that, at least in the Pomeron-dominated production processes, the generation of a new singularity is strongly disturbed through the presence of absorptive cuts. As shown in (5.17), in the absence of cuts one can, with an appropriate coupling U, promote the new singularity as much as one likes. But in the presence of cuts, this is no longer the case, because, at least for a certain range of values for U, we now have no new singularity at all. In this section we will address ourselves to the question whether the influence of cuts is always that strong. We will examine this in a model of multiparticle production, in which only one secondary trajectory (henceforth called Reggeon) couples to the produced particles. Absorptive effects are taken into account by allowing the rescattering Pomeron to couple to the Reggeon and to itself (again we take only fully enhanced diagrams). Rather than computing the production amplitude, we again turn directly to the cross sections and make use of the formalism developed in Sec. III. The diagrams that we are going to study are shown in Fig. 23. We recognize the following three renormalization effects: (i) The Pomeron propagator becomes renormalized, and this happens just in the same way as in the pure Pomeron theory. (ii) The Reggeon propagator gets renormalized,[32] and this renormalization is independent of the particle production. Hence, we can use the results of Abarbanel and Sugar[31] who have investigated the interaction between a Reggeon and the Pomeron. (iii) The RPR vertex undergoes renormalization. This is the only quantity that we will have to compute.

We take the Lagrangian

$$\mathfrak{L} = \sum_{i=1,2} \mathfrak{L}_i - U_0 \phi_1^\dagger \phi_1 \phi_2^\dagger \phi_2 + J^\dagger \phi_1^\dagger \phi_2^\dagger + J \phi_1 \phi_2, \quad (7.1)$$

with [cf. (3.3) for the Pomeron part]

$$\mathfrak{L}_i = \frac{i}{2}\psi_i^\dagger \overleftrightarrow{\partial}_t \psi_i - \alpha_0' \nabla\psi_i^\dagger \cdot \nabla\psi_i - \Delta_0 \psi_i^\dagger \psi_i - \frac{ig_0}{2}\psi_i^\dagger \psi_i(\psi_i + \psi_i^\dagger)$$
$$+ \frac{i}{2}\phi_i^\dagger \overleftrightarrow{\partial}_t \phi_i - \alpha_{R_0}' \nabla\phi_i^\dagger \cdot \nabla\phi_i - [1 - \alpha_R(0)]\phi_i^\dagger \phi_i - \frac{ir_0}{2}\phi_i^\dagger \phi_i(\psi_i + \psi_i^\dagger). \quad (7.2)$$

Here ψ_i, ϕ_i are the field operators of the Pomerons and Reggeons, respectively. Shifting the Reggeon energy by the substitution

$$\phi_i \to e^{i[1-\alpha_R(0)]t}\phi_i \quad (7.3)$$

we eliminate the term $[1 - \alpha_R(0)]\phi_i^\dagger \phi_i$ in $\mathfrak{L}_i$, i.e., we shift the Reggeon intercept to zero. This is possible only because the Reggeon number is conserved.

Now we can proceed in the same way as we did for the Pomeron and examine the infrared behavior of $\sigma_n(E)$, which is related to $\sigma_n(Y)$ via

$$\sigma_n(Y) = S^{2\alpha_R(0)-2}\frac{1}{2\pi i}\int dE e^{-EY}\sigma_n(E). \quad (7.4)$$

The key point is again the infrared behavior of the quartic coupling U. Defining the dimensionless coupling U by

$$U = \frac{U_d E_N^{D/2-1}}{(\alpha_R')^{D/2}}, \tag{7.5}$$

we obtain for the β_U function

$$\beta_U = r_R U + O(U^2), \tag{7.6}$$

with

$$r_R = \frac{D}{2} - 1 - \frac{D}{2}\frac{h}{\alpha_R'} + 2\gamma_{1R} + 2\gamma_{4R}, \tag{7.7}$$

in analogy to (4.48) with γ_{1R}, γ_{4R} being the anomalous dimensions of the Reggeon propagator and RPR vertex, respectively, and

$$h = E_N \partial_{E_N} \alpha_R'(E_N). \tag{7.8}$$

Calculating γ_{1R} and γ_{4R} in the manner outlined in Sec. IV A, we observe that these two quantities are closely related to each other. In fact we have

$$\gamma_{1R} + \gamma_{4R} = 0 \tag{7.9}$$

in all orders of perturbation theory. This follows very simply from a "Ward" identity that relates the RPR vertex to the Reggeon propagator[33]:

$$\Gamma_{RPR;\,\mathrm{unren}}(E_1, E_1, \vec{k}_1, \vec{k}_1) = \left.\frac{d\Gamma^{\mathrm{Reggeon}}_{\mathrm{unren}}(E, \vec{k}_1)}{dE}\right|_{E=E_1}. \tag{7.10}$$

Here $\Gamma^{\mathrm{Reggeon}}$ is the inverse Reggeon propagator, and (7.10) is easily understood by looking at graphs that contribute to Γ_{RPR} and the self-energy of the Reggeon. The "Ward" identity (7.10) is a consequence of the fact that in our theory the number of Reggeons is conserved at each vertex and that all produced particles couple to the Reggeon. In a theory with a triple-Reggeon coupling or in the pure Pomeron case there is no "Ward" identity. Formula (7.10) together with the definition of γ_{1R} and γ_{4R},

$$\Gamma_{RPR} = Z_{4R}^{-1}\Gamma_{RPR;\,\mathrm{unren}}, \tag{7.11}$$

$$\Gamma_{RPR}(E_1, E_2, \vec{k}_1, \vec{k}_2)\Big|_{\substack{E_1=E_2=-E_N \\ \vec{k}_1=\vec{k}_2=0}} = 1, \tag{7.12}$$

$$\Gamma^{\mathrm{Reggeon}} = Z_{1R}\Gamma^{\mathrm{Reggeon}}_{\mathrm{unren}}, \tag{7.13}$$

$$\frac{d}{dE}\, i\,\Gamma^{\mathrm{Reggeon}}(E, \vec{k})\Big|_{\substack{E=-E_N \\ \vec{k}=0}} = 1, \tag{7.14}$$

$$\gamma_{1R} = E_N \partial_{E_N} \ln Z_{1R}, \tag{7.15}$$

$$\gamma_{4R} = E_N \partial_{E_N} \ln Z_{4R} \tag{7.16}$$

leads directly to (7.9). We then find that in (7.7) the anomalous dimension associated with the Reggeon propagator is cancelled by the screening of the production vertex to all orders of perturbation theory. Finally, we have to determine the function h in (7.7), (7.8). It is the function which in the RGE for the Reggeon propagator determines the infrared behavior of the renormalized Reggeon slope (the analog to ξ for the Pomeron). If the renormalized Reggeon trajectory is to remain linear near $t=0$, then h, evaluated at the fixed-point values for all coupling constants, has to vanish. In fact, Abarbanel and Sugar found a solution to the Reggeon-Pomeron interaction, where the renormalized Reggeon trajectory is linear near $t=0$, and the value of h corresponding to this solution, is zero in their approximation (first-order ϵ expansion).[34] We expect that if this linear solution survives in higher-order ϵ, then h will remain zero. Therefore, the coefficient r_R of U in (7.7) vanishes at $D=2$, unlike the Pomeron case (4.47), where $r \neq 0$. This is a nonperturbative result.

As a result of this, the function $U(t)$ will have a different form than in the Pomeron case (4.50), where r was nonzero. In the present case

$$\beta_U = aU^2 + O(U^3), \tag{7.17}$$

and a must be negative. To prove this, let us assume that $a>0$. Then $U=0$ is an infrared-stable fixed point, and $U(-t)$ has the form

$$U(-t) = \frac{U}{1-aUt}. \tag{7.18}$$

We stated in Sec. IV (4.58) and (4.59) that this leads to

$$\tilde{\sigma}_{n+2}(\omega) \sim \omega^{2\gamma_R - 1 + D/2}(\ln\omega)^n. \tag{7.19}$$

However, a closer look at the coefficient of $\tilde{\sigma}_{n+2}$ teaches us that, for $a>0$, the sign alternates as a function of n. Thus, positivity of the cross sections, which is an input into the construction of RFT for σ_n, tells us that (7.18) with $a>0$ is not possible. So let us take $a<0$, and assume that β_U has no higher terms. Then (7.18) is the exact behavior of $U(t)$ and (7.19) that of $\tilde{\sigma}_n$. Furthermore, (7.18) indicates the existence of a pole at $t = 1/aU$. Finally, if β_U in (7.17) has further terms that lead to a second zero of β, then this zero at $\bar{U}$ is infrared stable and $U(t)$ gets driven to that point:

$$U(t) \underset{t\to\infty}{\sim} \bar{U} + (U - \bar{U})e^{-bt}, \tag{7.20}$$

where b is the slope of β_U at $\bar{U}$. With this we go back into (4.49) and again find a behavior like (7.19). We, therefore, conclude that (7.19) describes the infrared behavior of $\tilde{\sigma}_n$, and this is a consequence of quite general arguments. Turning to the Y behavior of $\sigma_n(Y)$, we find

$$\sigma_{n+2}(Y) \sim s^{2\alpha_R(0)-2} \frac{(\ln Y)^n}{Y} (\ln Y)^{-2\gamma_R} U^n . \qquad (7.21)$$

This result is the analog to (4.57) for the Pomeron-dominated production processes. Except for the n-independent power of $\ln Y$, it has the same structure as our simple model in Sec. II with $p=0$, i.e., the Finkelstein-Kajantie model. This comes about because the screening of the RPR vertex (anomalous dimension γ_{4R}) is just enough to cancel the anomalous dimension of the renormalized Reggeon propagator (γ_{1R}). What then remains is the shrinkage, and since we have used the linear solution for the Reggeon, our result is practically the same as one would obtain in a model without Pomeron cuts. The dominant contributions to $\sigma_n(Y)$ are due to that kinematic configuration where all rapidity gaps are large (and not only one as it was the case for Pomeron exchange).

We thus have established that the effect of Pomeron cuts in those multiparticle production processes which are described by a secondary Reggeon exchange is considerably weaker than in Pomeron-dominated processes. In fact, the qualitative behavior of $\sigma_n(Y)$ is practically unchanged in the presence of cuts. As a consequence, the mechanism of generating a new j-plane singularity is not disturbed, and these processes can, even in the presence of cuts, serve as a candidate for building the Pomeron singularity.

We finally want to relate our results to some other work along this line that has been done recently.[6,35-37] The effect of absorption in multiparticle production from a secondary Regge pole has been studied by Ciafaloni and Marchesini.[6] For $\sigma_n(Y)$ they find a result which is similar to ours (7.16). Compared to their calculations which are motivated by an s-channel absorptive picture, our calculations are more complete from the point of view of t-channel unitarity. In particular, they do not consider self-interactions of the absorbing Pomeron or renormalization of the Reggeon propagator. That the conclusions are the same, despite the different frameworks of calculations, means that the character of a secondary Reggeon is quite insensitive with respect to absorption by the Pomeron.

Having established that the presence of Pomeron cuts does not destroy the mechanism of generating a new singularity in $\sigma(E)$ and assuming that, for an appropriate value of the RPR coupling, this singularity corresponds to the Pomeron, one might ask whether these processes can account not only for the correct *position* of the singularity, but also for the *power of* ($\ln s$) that are required for σ_{tot} in RFT. Within our calculations, an answer to this requires a study of the nature of this singularity [if it is a simple pole, no ($\ln s$) factors would arise], and our knowledge of the β_U function is not sufficient for this purpose. On the other hand, Caneschi and Jengo[35] have studied absorptive corrections to the cut Pomeron, and identifying this with the singularity built up by multiparticle production processes, their results may shed some light on this question. They claim that they can construct a solution which yields the same behavior of the total cross section as that derived from the study of $2 \to 2$ processes.

VIII. SUMMARY

In this paper we have confronted RFT with one of the most serious tests of s-channel unitarity that have failed in the past for Pomeron-pole models. The constraint we have studied is that following from multiparticle production. We find that, in the presence of cuts, processes with repeated Pomeron exchange no longer violate the Froissart bound, provided the $\tilde{P}P\tilde{P}$ coupling is not too large. However, we qualify this result by giving some indication that a two-Pomeron bound state of $j>1$ can still be formed, if one takes the $\tilde{P}P\tilde{P}$ coupling large enough. We do not know whether such a bound state can be eliminated by other types of production processes, or whether its possible existence imposes a restriction on the value of the $\tilde{P}P\tilde{P}$ vertex.

In the process of preserving s-channel unitarity all $\sigma_n(s)$ are forced to behave asymptotically like σ_{el}, the physical picture emerging from this being that mainly only one large rapidity gap is opened between the produced particles. The rapidity distribution of a single event will, therefore, exhibit large fluctuations. This is in agreement with the idea that particle production at high energies resembles a system being at a phase transition.

The basic mechanism by which violation of s-channel unitarity is prevented is the screening of the $\tilde{P}P\tilde{P}$ vertex. By opening this vertex and studying the $\tilde{P}PR$ vertex at nonzero Reggeon momentum we show that decoupling problems do not arise.

We then pointed out that in the case of particle production by a secondary Regge pole the presence of Pomeron cuts does not lead to as drastic changes as in the Pomeron-dominated processes. Namely, the qualitative behavior of $\sigma_n(s)$ remains essentially unchanged once cuts are included, and the produced particles have still a uniform rapidity distribution. This indicates that even in the presence of cuts these processes can generate a new singularity which can be promoted

for any finite coupling.

In this paper we have mainly been concerned with the question whether RFT with a Pomeron whose intercept is 1 passes a strong test imposed by s-channel unitarity. But at the same time we have gained some insight into the mechanism in which the bare Pomeron might be built up. One of the most important questions that have to be asked in the future is why the Pomeron singularities actually are at 1. It has been suggested that this reflects an underlying structure of hadrons and hadron dynamics. But it is also possible that the full content of s-channel unitarity does not allow for a Pomeron intercept other than 1. We hope that our results might be of some help for future investigations along this line.

ACKNOWLEDGMENTS

For helpful discussions we would like to thank H. D. I. Abarbanel, J. Carazzone, J. Cardy, S. D. Ellis, and A. Schwimmer.

APPENDIX

In this Appendix we will study in detail the β_U function [defined in Eq. (4.41)] near $D=4$. The Lagrangian we use is defined in (3.10) together with (5.19). Our main interest is to show that near $D=4$ the structure of β_U is nearly unchanged through the presence of the triple-Pomeron interaction and that the results holding in the absence of the Pomeron self-interaction carry over. To this end we compute β_U (which is a function of U, a, and g^2) up to order g^2 and U^2.

The Lagrangian in (5.19) contains, in addition to the parameters whose renormalization has been described in Sec. IV, the new parameter a_0. Following Ref. 26 we define

$$-\frac{1}{2\alpha'}\left(\frac{\partial}{\partial k^2}\right)^2 i\,\Gamma^{11}(E,k^2,\alpha',g,a,E_N)\Big|_{E=E_N=a_d,\ k^2=0}, \tag{A1}$$

and introduce its dimensionless version

$$a=\frac{E_N}{\alpha'}\,a_d. \tag{A2}$$

The RGE for any Green's function contains an additional β function which describes the change of a as a function of E_N:

$$\beta_a(g,a)=E_N\partial_{E_N}a(E_N). \tag{A3}$$

To first order in ϵ, β_a is[26]

$$\beta_a=a-\frac{g^2}{64\pi}, \tag{A4}$$

and β_g and ζ/α' are the same as in the theory without the k^4 term in the Pomeron trajectory. The function β_U has the form

$$\beta_U=-r(g^2)U-C(g^2,a)U^2 \tag{A5}$$

with r from (4.47).

Before we turn to the actual computation of $C(g^2,a)$ we note the following. In order to solve the RGE for any Green's function (e.g., Γ^{22}) we search for the solution of the auxiliary functions

$$\frac{dg(t)}{dt}=-\beta_g(g(t),a(t)),\quad g(0)=g, \tag{A6}$$

$$\frac{da(t)}{dt}=-\beta_a(g(t)^2,a(t)),\quad a(0)=a, \tag{A7}$$

$$\frac{dU(t)}{dt}=-\beta_U(U(t),g(t)^2,a(t)),\quad U(0)=U. \tag{A8}$$

In first order ϵ, β_g does not depend on a and we, therefore, solve successively (A6), and (A7) and obtain for $U(t)$

$$\frac{dU}{dt}=-rU+\tilde{C}(t)U^2. \tag{A9}$$

[r is also a function of t, but we know that for large t it approaches the constant, (4.48), and we are interested in the solution to (A9) for large t.] The solution to (A9) is

$$U(t)=\frac{e^{-rt}}{1/U-I(t)}, \tag{A10}$$

with

$$I(t)=\int_0^t dt'e^{-t'}C(t')\,dt'. \tag{A11}$$

As long as $I(\infty)$ is positive and finite, we have

$$0<I(\infty)<\infty, \tag{A12}$$

$$U_c=1/I(\infty), \tag{A13}$$

such that, for $U_c<U$, $U(t)$ in (A10) encounters a pole.

We, therefore, have to show that (A12) is, indeed, satisfied in our theory. The graphs which contribute to $C(g^2,a)$ in (A5) are shown in Fig. 24. Let us first take $D=4$. Then we know that

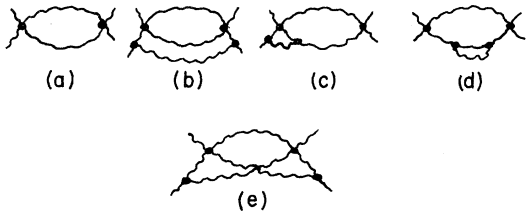

FIG. 24. Diagrams contributing to β_U, which are of second order in U and up to first order in g^2.

$$\beta_g = K_1 g^3, \quad K_1 > 0 \tag{A14}$$

and

$$g^2(t) = \frac{1}{1/g^2 + K_1 t}. \tag{A15}$$

From (A4) and (A7) we obtain

$$a(t) = e^{-t}\left[a + K_2 \int_0^t \frac{e^{t'}}{1/g^2 + K_1 t'}\, dt'\right] \quad (K_2 > 0) \tag{A16}$$

i.e., for large t

$$a(t) \sim \frac{K_2}{K_1}\frac{1}{t}. \tag{A17}$$

For small a, the contribution of Fig. 24(a) to $C(g^2, a)$ is of the form $\ln(1/a) \times$(positive constant), i.e., with (A17)

$$\tilde{C}(t) \sim \ln t \times \text{positive constant}. \tag{A18}$$

All other graphs of Fig. 24(a) yield contributions of the form $g^2 \ln^2 t$, but since $g^2 \sim 1/t$ [from (A15)] they are much smaller than (A18). Hence, Fig. 24(a) gives the leading contribution, and inserting (A18) into (A11) we find that indeed (A12) is satisfied. When $D \neq 4$, g^2 is of the order $\epsilon = 4 - D$ and Figs. 24(b)–24(c) yield contributions to $\tilde{C}(t)$ of the order ϵ. Therefore, for small ϵ, Fig. 24(a) still gives the leading term whose large-t behavior is now

$$\tilde{C}(t) \sim \text{const} > 0. \tag{A19}$$

Again, (A12) is satisfied. This demonstrates that near $D = 4$ the presence of $\tilde{P}$ cuts does, indeed, not affect the existence of a pole in $U(t)$ for $U > U_C$.

---

*Address after 1 October 1975: II. Institut für Theor - etische Physik, University of Hamburg, Hamburg, West Germany.

†Operated by Universities Research Association, Inc. under contract with the Energy Research and Development Administration.

[1]A. A. Migdal, A. M. Polyakov, and K. A. Ter-Martirosyan, Phys. Lett. 48B, 239 (1974); Zh. Eksp. Teor. Fiz. 67, 848 (1974) [Sov. Phys. JETP 40, 420 (1974)].

[2]H. D. I. Abarbanel and J. B. Bronzan, Phys. Lett. 48B, 345 (1974); Phys. Rev. D 9, 2397 (1974).

[3]A comprehensive review of RFT is given by H. D. I. Abarbanel, J. B. Bronzan, R. L. Sugar, and A. R. White, Phys. Rev. 21C, 119 (1975).

[4]J. Finkelstein and M. Jacob, Nuovo Cimento 56A, 681 (1968); L. Caneschi, Phys. Rev. Lett. 23, 254 (1969).

[5]J. Finkelstein and F. Zachariasen, Phys. Lett. 34B, 631 (1971); L. Caneschi and A. Schwimmer, Nucl. Phys. B44, 631 (1972).

[6]M. Ciafaloni and G. Marchesini, Nucl. Phys. B88, 109 (1975).

[7]A review of Pomeron decoupling theorems is contained in R. C. Brower, C. E. DeTar, and J. H. Weis, Phys. Rep. 14C, 257 (1974); R. C. Brower and J. H. Weis, Rev. Mod. Phys. 47, 605 (1975).

[8]H. D. I. Abarbanel, J. Bartels, J. B. Bronzan, and D. Sidhu, Phys. Rev. D 12, 2459 (1975); 12, 2798 (1975).

[9]Some other s-channel unitarity tests of RFT have been considered by J. L. Cardy, Santa Barbara report, 1975 (unpublished).

[10]I. A. Veriev, O. V. Kanchell, S. G. Martinyan, A. M. Popova, and K. A. Ter-Martirosyan, Zh. Eksp. Teor. Fix. 46, 1700 (1964) [Sov. Phys. JETP 19, 1146 (1964)]

[11]J. Finkelstein and K. Kajantie, Nuovo Cimento 56A, 659 (1968); Phys. Lett. 26B, 305 (1968).

[12]J. Bartels, Phys. Rev. D 11, 2977 (1975); 11, 2989 (1975).

[13]R. L. Sugar and A. R. White, Phys. Rev. D 10, 4063 (1974); 10, 4074 (1974).

[14]A similar language has been used by L. Caneschi, Nucl. Phys. B35, 406 (1971).

[15]R. C. Brower and J. H. Weis, Phys. Lett. 41B, 631 (1972). See also Ref. 7.

[16]V. N. Gribov, Zh. Eksp. Teor. Fiz. 53, 654 (1967) [Sov. Phys. JETP 26, 414 (1968)].

[17]W. Zimmermann, in *Lectures on Elementary Particles and Quantum Field Theory*, 1970 Brandeis University Summer Institute in Theoretical Physics, edited by S. Deser, M. Grisaru, and H. Pendleton (MIT Press, Cambridge, Mass., 1970), Vol. 1, p. 395.

[18]Contributions, where two or more Pomerons couple to the incoming particles at the right and left end of Fig. 12, are down by powers of $\ln s = Y$. This can be shown in the same fashion as for the $2 \to 2$ scattering (Ref. 2) or for the triple-Regge region (Ref. 8).

[19]J. Ellis and R. Savit, Nucl. Phys. B94, 477 (1975).

[20]Jan W. Dash and S. J. Harrington, Oregon Report No. OITS-75-2, 1975 (unpublished).

[21]H. D. I. Abarbanel and J. B. Bronzan, Phys. Rev. D 9, 3304 (1974).

[22]W. A. Bardeen, J. W. Dash, S. S. Pinsky, and V.Rabl, Phys. Rev. D 12, 1820 (1975).

[23]R. C. Brower, J. Ellis. R. Savit, and W. J. Zakrzewski, Nucl. Phys. B94, 460 (1975).

[24]J. L. Cardy and R. L. Sugar, Phys. Rev. D 12, 2514 (1975).

[25]D. J. Gross and A. Neveu, Phys. Rev. D 10, 3235 (1974). See also D. J. Gross and F. Wilczek, *ibid.* 8, 3633 (1973).

[26]R. C. Brower and J. Ellis, Phys. Lett. 51B, 242 (1974).

[27]V. A. Abramovskiĭ, V. N. Gribov, and O. V. Kancheli, Yad. Fiz. 18, 595 (1973) [Sov. J. Nucl. Phys. 18, 308 (1974)].

[28]C. E. Jones, F. E. Low, S. H.-H Tye, G. Veneziano, and J. E. Young, Phys. Rev. D 6, 1033 (1972).

[29]D. I. Olive and J. C. Polkinghorne, Phys. Rev. 171, 1475 (1968).

[30]R. J. Eden, P. V. Landshoff, D. I. Olive, and J. C. Polkinghorne, in *The Analytic S-Matrix* (Cambridge Univ. Press, New York, 1966), Chapter II.

[31]H. D. I. Abarbanel and R. L. Sugar, Phys. Rev. D 10, 721 (1974).
[32]In a recent paper, A. Schwimmer and F. Zachariasen [Phys. Lett. 57B, 357 (1975)] point out that a secondary Reggeon should be renormalized in a different way.
[33]A. A. Ansel'm and I. T. Dyatlov, Zh. Eksp. Teor. Fiz. 54, 1001 (1968) [Sov. Phys. JETP 27, 533 (1968)].
[34]In defining h, we have left the notation of Abarbanel and Sugar of Ref. 31. When expressed in terms of their notation, we have $h/\alpha_R{}' = \sigma/\nu + \zeta/\alpha'$.
[35]L. Caneschi and R. Jengo, Nucl. Phys. B89, 19 (1975).
[36]P. Suranyi, Phys. Rev. D 12, 2124 (1975).
[37]M. Ciafaloni and G. Marchesini, Phys. Lett. 55B, 471 (1975).